DIELECTRIC AND OPTICAL STUDY OF $KTa_xNb_{1-x}O_3$ MIXED CRYSTALS

by

LEE TROVER TODD, Jr.

B.S., University of Kentucky
(1968)

SUBMITTED IN PARTIAL FULFILLMENT OF THE

REQUIREMENTS FOR THE DEGREE OF

MASTER OF SCIENCE

at the

MASSACHUSETTS INSTITUTE OF TECHNOLOGY

June, 1970

Signature of Author .. ..
Department of Electrical Engineering, June 4, 1970

Certified by .....
Thesis Supervisor

Accepted by .....
Chairman, Department Committee on Graduate Students

DIELECTRIC AND OPTICAL STUDY OF $KTa_xNb_{1-x}O_3$ MIXED CRYSTALS

by

LEE TROVER TODD, Jr.

Submitted to the Department of Electrical Engineering on June 4, 1970, in partial fulfillment of the requirements for the Degree of Master of Science.

ABSTRACT

Mixed crystals in the $KTa_xNb_{1-x}O_3$ system have been grown with compositions ranging from $KTaO_3$ to 60% $KNbO_3$. The dielectric phase diagram has been determined for the composition range 4% to 40% $KNbO_3$. The three transition temperatures become closer together with decreasing $KNbO_3$ concentration. For crystals containing less than 5% $KNbO_3$, only one transition was observed.

The polarization dependence of the small signal dielectric constant was measured using a low duty factor AC bias technique. The fourth-order polarization coefficient in the Devonshire free energy expansion was determined for five compositions. For crystals containing less than 30% $KNbO_3$, this coefficient was positive, indicating a second-order paraelectric-to-ferroelectric phase transition. Crystals containing greater than 30% $KNbO_3$ exhibited first-order transitions. The fourth-order polarization coefficient varies almost linearly with temperature over about a ten to twelve degree range above the paraelectric-to-ferroelectric transition. For higher temperatures, it saturates to approximately a constant value.

Raman scattering was observed in crystals with compositions between 6% and 33% $KNbO_3$. No first-order Raman spectrum was observed in the paraelectric phase. The ferroelectric "soft" mode was overdamped in the tetragonal and orthorhombic phases of all crystals observed. In the rhombohedral phase, this mode was underdamped for crystals containing less than 27% $KNbO_3$ and was overdamped for crystals containing more than 33% $KNbO_3$, suggesting a strong correlation between the damping of the ferroelectric mode and the thermodynamic order of the paraelectric-to-ferroelectric transition.

Thesis Supervisor: Thomas G. Davis

Title: Assistant Professor of Electrical Engineering

ACKNOWLEDGMENTS

The author would like to express his appreciation to Professor T. G. Davis for his supervision of this thesis and for numerous helpful discussions throughout the work. He would also like to thank Professor A. Smakula and Dr. A. Linz for providing the facilities necessary for this research.

The author is grateful to Mr. V. Belruss for growing the crystals required for the investigation and to Dr. D. Gabbe for the chemical analysis of these crystals. Also, he would like to express his gratitude to the other members of the Crystal Physics Laboratory who assisted in various phases of the investigation, particularly to J. Kalnajs, R. Mills, E. Farrell and A. Vetrovs.

The personal financial support provided by the John and Fannie Hertz Foundation during this period of study is also greatly appreciated.

Finally, the author is most grateful to Miss Aina Sils for typing this thesis; to Mr. J. Mara for drawing the illustrations; and to his wife for her patience and concern during this work.

TABLE OF CONTENTS

LIST OF ILLUSTRATIONS

Figure

I. INTRODUCTION

1. Ferroelectricity

A ferroelectric is a material which possesses a spontaneous polarization that can be reversed by the application of an appropriate electric field. The polarization and the electric field are related by a hysteresis loop which is characteristic of a material in a ferroelectric phase. Ferroelectricity usually disappears above a certain temperature called the transition temperature. Above the transition the crystal is said to be in the paraelectric phase where the dielectric constant usually obeys a Curie-Weiss law,

$$\varepsilon = C/(T - T_o), \tag{1}$$

where C is the Curie constant and T_o, the Curie-Weiss temperature, is either the transition temperature or just a few degrees below it. The dielectric constant falls off rapidly below the transition.

Ferroelectrics can be grouped into two classes according to the nature of the phase change occurring at the transition. The first group is characterized by the existence of permanent dipole moments in the polar and nonpolar phases. In the nonpolar phase, the dipole moments are randomly oriented and thus do not produce a net polarization. These dipole moments do, however, become ordered below a certain critical temperature and give rise to the spontaneous polarization. This is then an order-disorder transition. In the second group, there are no permanent dipole moments in the nonpolar phase and the crystal undergoes a displacive transition. At the transition,

the lattice deforms in such a way that the positive sublattice is displaced relative to the negative sublattice and a spontaneous polarization results.

The phase transition can also be classified thermodynamically as either first- or second-order. For a first-order transition there is a latent heat and the spontaneous polarization is discontinuous at the transition temperature. A second-order transition is characterized by no latent heat and a continuous spontaneous polarization.

The simplest structure known to be ferroelectric is the perovskite structure (Fig. 1). Ferroelectric crystals of this structure have a general chemical formula ABO_3, where the A atoms are on the cube corners, the B atom is in the center of the cube and the O atoms are at the face centers. Ferroelectrics with this structure undergo displacive-type transitions which can be either first- or second-order. These perovskite ferroelectrics have received considerable attention in the study of ferroelectricity due to their simple structure.

The onset of ferroelectricity can be discussed from two related viewpoints. The first is the "polarizability catastrophe" in which for some critical condition the lattice polarizability becomes very large. To see how this might occur, consider the case of a cubic lattice of point ions, all having a polarizability α. The field at each lattice site is equal to the applied field E_a plus the field due to the dipole fields of the other ions. The field at a lattice point, in a simple cubic lattice, due to the

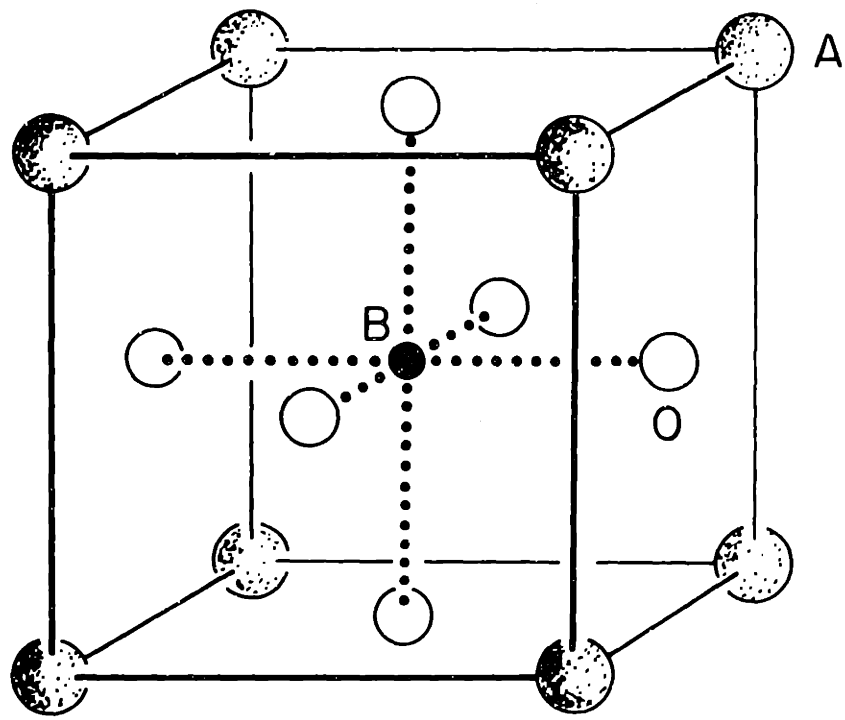

Fig. 1. Perovskite structure.

other dipoles is given by $P/3\epsilon_o$ (M.K.S.), where P is the macroscopic polarization of the lattice. If there are N atoms per unit volume, the total polarization is

$$P = N\alpha(E_a + P/3\epsilon_o). \tag{2}$$

Solving this for P,

$$P/E_a = N\alpha/(1 - N\alpha/3\epsilon_o). \tag{3}$$

Therefore, when $N\alpha/3\epsilon_o$ approaches unity, P/E_a approaches infinity, and there can be a finite polarization with no applied field, i.e., a spontaneous polarization. This is the approach which was taken by Slater[1] in his treatment of $BaTiO_3$.

The second viewpoint relates the ferroelectric transition to a transverse optical phonon mode frequency which assumes unusually low values at the transition temperature. The theory, developed by Anderson[2] and Cochran,[3] takes into consideration the normal vibrational modes and their relation to the ferroelectric behavior of the crystal. They find that for one particular mode, at a certain temperature, the short-range restoring forces and the long-range Coulomb forces almost cancel. The total restoring force is then very small and the crystal becomes unstable for that particular mode. This is called the "ferroelectric soft mode" because, according to Cochran, it is responsible for the ferroelectric behavior of the crystal.

These two viewpoints are related by the Lyddane-Sachs-Teller[4] relation:

$$\frac{\varepsilon_s}{\varepsilon_\infty} = \left(\frac{\omega_{LO}}{\omega_{TO}} \right)^2 . \qquad (4)$$

From this, the unusually high dielectric constant in the polarizability catastrophe theory occurs due to the unusually low value of one of the transverse optical mode frequencies as predicted by the Cochran theory.

2. Problem Definition

The ferroelectric soft mode has been observed by several experimentalists using Raman scattering. The soft mode in $BaTiO_3$[5] and $KNbO_3$, ferroelectrics with first-order paraelectric to ferroelectric transitions, is overdamped while this mode in $(K,Na)TaO_3$,[6] a crystal system with a second-order phase transition, is underdamped.

The purpose of this study is to investigate the correlation, if any, between the order of the phase transition and the damping of the ferroelectric mode. To do this, it is desirable to have a crystal system which has a first-order transition for some compositions and a second-order transition for the remaining compositions. $KTa_xNb_{1-x}O_3$, or KTN, is a crystal system with this property. It will be necessary to find the composition at which the phase transition changes from first- to second-order and then observe the Raman scattering spectra for crystals with compositions above and below this critical composition.

The dielectric properties of KTN have been studied by several authors.[7-9] Kurtz[10] and Triebwasser[7] report values of 33 and 45 mole %

$KNbO_3$, respectively, as the composition at which the transition changes from first- to second-order. The large discrepancy in their results and the manner in which they determined their respective values leads to the belief that neither of these values is accurate. Raman scattering spectra of KTN have been observed[11] but the ferroelectric mode could not be resolved. This is, then, the first study of the ferroelectric mode in KTN and also the first study of a possible correlation between the damping of the ferroelectric mode and the order of the phase transition.

3. Dielectric and Structural Properties of KTN

The KTN system is composed of the two end members, $KNbO_3$ and $KTaO_3$. $KNbO_3$ is ferroelectric below 708°K.[12] Its dielectric properties have been studied by Matthias and Remeika,[12] Shirane et al.,[13] and Triebwasser,[14] while its crystal structure has been reported by Wood,[15] Vousden,[16] and Shirane et al.[13] In Fig. 1, the A atoms correspond to potassium; the B atom, to niobium; and the O atoms to the oxygen atoms in $KNbO_3$. $KNbO_3$ is cubic above 708°K with lattice parameter 4.024 Å[16] at 770°K and then becomes tetragonal. At 498°K its structure changes to orthorhombic and remains so until 228°K where it becomes rhombohedral. All three of these transitions are first-order.[13,17]

The dielectric properties of $KTaO_3$ have been studied by several authors.[18-21] Hulm et al.[18] reported a transition to a ferroelectric state at 13°K. Later, Wemple,[19] using higher purity crystals, found that no transition to a ferroelectric state took place above liquid helium temperature. The room temperature structure of $KTaO_3$ is cubic

perovskite with a lattice parameter 3.989 Å.[16] In Fig. 1, the A atoms again correspond to potassium; the B atom, to tantalum; and the O atoms to the oxygen atoms in $KTaO_3$. The structure probably remains cubic at lower temperatures but a low-temperature study does not appear to have been conducted.

The dielectric properties of KTN were first studied by Triebwasser[7] in the composition range 20 to 100 mole % $KNbO_3$ in the temperature interval 90° to 720°K. His results indicate the following:

1) The paraelectric-to-ferroelectric transition temperature (Curie temperature) moves to lower temperatures with decreasing $KNbO_3$ concentration.

2) The peak dielectric constant decreases with decreasing $KNbO_3$ concentration.

3) The thermal hysteresis of the transition temperatures decreases with decreasing $KNbO_3$ concentration.

Triebwasser's data also indicated that the paraelectric-to-ferroelectric transition changed from first-order to second-order at approximately 45 mole % $KNbO_3$ with higher $KNbO_3$ concentrations giving first-order transitions and lower concentrations, giving second-order transitions.

More recent dielectric measurements of KTN have been reported by Chen et al.[8] They have measured the Devonshire coefficients (see section on thermodynamics) for two compositions of the KTN system. The fourth-order polarization coefficient allows the determination of

the order of the paraelectric-to-ferroelectric transition. Using their data and a value of the fourth-order polarization coefficient determined by Kahng and Wemple[21] for $KTaO_3$, Kurtz[10] reports a value of the composition at which the transition changes from first- to second-order of about 33 mole % $KNbO_3$. Wemple et al.[9] have also measured the Devonshire coefficients using measurements obtained from surface barrier junctions formed on semiconducting crystals of KTN. Their values differed considerably from those obtained by Chen et al.[8] possibly due to clamping effects associated with the surface junction geometry.

The structural properties of the KTN system have also been reported by Triebwasser.[7] KTN undergoes the same sequence of structure changes as $KNbO_3$ in the composition range 20 to 100 mole % $KNbO_3$. A structural study of compositions below 20 mole % $KNbO_3$ does not appear to have been conducted.

II. THEORETICAL CONSIDERATIONS

1. Thermodynamic Theory of Ferroelectrics

Many properties of ferroelectrics such as polarization and dielectric constant, as well as their temperature, field, and pressure dependence, can be interrelated through a thermodynamic formalism developed by Devonshire.[22] This formalism can be used to develop a method for determining the order of the ferroelectric transition from the polarization dependence of the dielectric constant. In this section, we will develop the equations essential to this determination.

The differential of the internal energy of a body subject to external stresses and electric field is

$$dU = TdS - \sum_{i=1}^{3} X_i dx_i + \vec{E}\cdot d\vec{P}, \tag{5}$$

where S is the entropy, T the temperature, x_i and X_i the strain and stress components, respectively, $\vec{E}$ the electric field and $\vec{P}$ the polarization. If the experiment is such that the external conditions are constant temperature and constant stress, the most convenient potential function to use is the elastic Gibbs function, G, obtained from U by two Legendre transformations:

$$G = U + \sum_{i=1}^{3} X_i x_i - TS, \tag{6}$$

with the corresponding differential

$$dG = -SdT + \sum_{i=1}^{3} x_i dX_i + \vec{E}\cdot d\vec{P}. \tag{7}$$

For the above external conditions, Eq. 7 becomes

$$dG = \underset{\rightarrow}{E} \cdot d\underset{\rightarrow}{P}. \tag{8}$$

If the stress is taken to be constant, G can be expanded in powers of the polarization with coefficients which depend only on temperature. If the crystal has a center of inversion above the Curie temperature, this expansion can be made in even powers of the polarization:

$$G = G_o + AP^2 + BP^4 + CP^6 + \cdots, \tag{9}$$

where, for simplicity, the polarization has been assumed to be directed along only one axis and G_o is the free energy for zero polarization. The basic assumption in this thermodynamic treatment is that Eq. 9 can be applied both above and below the transition.

From Eq. 8,

$$E = \left(\frac{\partial G}{\partial P}\right)_{T,X} = 2AP + 4BP^3 + 6CP^5 + \cdots. \tag{10}$$

Also,

$$\left(\frac{\partial E}{\partial P}\right)_{T,X} = \frac{1}{\varepsilon - \varepsilon_o} \sim \frac{1}{\varepsilon} = 2A + 12BP^2 + 30CP^4 + \cdots, \tag{11}$$

where A, B and C are the temperature-dependent coefficients and the approximation in Eq. 11 is valid since, for ferroelectrics in the vicinity of the transition, ε is of the order of $10^4\ \varepsilon_o$. For Curie-Weiss behavior in the paraelectric phase, we require that A have the form

$$A = A'(T - T_o), \tag{12}$$

where A' is independent of temperature and T_o is the Curie-Weiss

temperature, not necessarily the transition temperature. A will then be positive or negative depending on the sample temperature.

The entropy may be obtained from the differential of G as

$$S = -\left(\frac{\partial G}{\partial T}\right)_{X,P} = S_o - \left(\frac{dA}{dT}\right)P^2 - \left(\frac{dB}{dT}\right)P^4 - \left(\frac{dC}{dT}\right)P^6 - \cdots. \qquad (13)$$

The entropy is then continuous or discontinuous at the transition temperature, depending upon whether or not the polarization is continuous. If the polarization, and therefore the entropy, is discontinuous at the transition, there is a latent heat, and the transition is said to be first-order. If the polarization is continuous, there is a discontinuity in the specific heat but no latent heat, and the transition is second-order.

From Eq. 9, one sees that G will be equal to $G_o(T)$ in the nonpolar phase and that this value will be a minimum at zero polarization since A is positive in the nonpolar phase. Therefore, the stable state for the system in the nonpolar phase is at zero polarization. As the temperature is decreased, the stable state of the system will change from one with the polarization equal to zero to one with nonzero polarization and the system will undergo a ferroelectric transition. The nature of the phase transition will depend on the signs of the coefficients in the free energy expansion. The simplest case occurs when A', B and C are positive and terms of higher order than P^6 are negligible in Eq. 9. The spontaneous polarization can be calculated by setting Eq. 10 equal to zero:

$$E = 0 = 2AP_s + 4BP_s^3 + 6CP_s^5. \qquad (10')$$

This equation has five solutions given by

$$P_s^2 = \frac{1}{6C}\left[-2B \pm \sqrt{4B^2 - 12AC}\right], \quad P_s = 0 \qquad (14a,14b)$$

The solutions of Eq. 14a corresponding to the minus sign can be neglected since they will always lead to imaginary values for P_s in the case of B and C positive. For A positive, Eq. 14a has no real solutions, so that the stable state of the system is at $P_s = 0$. When $A = 0$, $P_s^2 = 0$ in Eq. 14a, and as A becomes negative, there are two real nonzero solutions for P_s corresponding to minima in the free energy. Thus the system changes from one with $P_s = 0$ to one with P_s nonzero and the system has undergone a ferroelectric transition. Since this change in P_s is a continuous function of A, and thus of temperature, the transition is second-order. Also, since the transition takes place at $A = 0$, $T_{tr} = T_o$, the Curie-Weiss temperature is equal to the transition temperature in the case of a second-order transition.

The next simplest case is one in which A' and C are positive, B is negative and terms of higher order than P^6 are again negligible in Eq. 9. In this case, the spontaneous polarization is again given by Eqs. 14a and 14b, but since B is negative, there will be five solutions in general even though A is positive. The two nonzero solutions in Eq. 14a corresponding to the minus sign will give maximum for the system and can be neglected in determining the stable state of the system. The condition for a transition is that the free energy at the nonzero values of polarization be equal to the free energy at zero polarization. Therefore, from Eq. 9,

$$G_p - G_o = 0 = AP_s^2 + BP_s^4 + CP_s^6, \qquad (15)$$

where G_P is the free energy at the nonzero value of polarization. Solving Eqs. 15 and 10' simultaneously for P_s, one finds

$$P_s^2 = -B/2C \tag{16}$$

as the value of the spontaneous polarization at the transition. Since, for this case, B is negative and C is positive, Eq. 16 gives real nonzero values of P_s. Thus the polarization changes discontinuously from zero to some nonzero value at the transition and the transition is first-order. From Eqs. 15 and 10', one can also solve for the value of A at the transition:

$$A = B^2/4C = A'(T_{tr} - T_o) > 0. \tag{17}$$

Therefore, in the case of a first-order transition, the transition temperature is higher than the Curie-Weiss temperature.

For these two simple cases, the order of the phase transition depends only on the sign of B. Therefore, a calculation of the value of B from experimental data provides a means of determining the order of the phase transition. From Eq. 11, neglecting terms of higher order than P^2, one finds

$$\frac{1}{\varepsilon} = 2A + 12BP^2. \tag{18}$$

If the lattice is polarized by an external field and the dielectric constant measured, a plot of Eq. 18 can be constructed. The slope of this plot will be proportional to B with a positive slope indicating a second-order transition and a negative slope, a first-order transition.

If the fourth-order term in Eq. 11 is not negligible, Eq. 18 will become

$$\frac{1}{\varepsilon} = 2A + 12BP^2 + 30CP^4. \tag{18'}$$

This additional term was taken into consideration in the theory above so that the transition can still be determined from the sign of B. A plot of $1/\varepsilon$ versus P^2 will have to be fitted to Eq. 18' to determine the values of A, B and C and thus the order of the transition.

If terms of order P^6 must be considered in Eq. 11, the determination of the order of the transition becomes much more difficult. This case was not encountered so it will not be considered in this section.

A method of determining Eq. 18 and Eq. 18' experimentally is discussed in the section on experimental techniques.

2. Microscopic Calculation of the Free Energy

While the thermodynamic theory of ferroelectricity is completely macroscopic, Slater's[1] treatment of $BaTiO_3$ allows the determination of the constants in the free energy expansion (Eq. 9) in terms of microscopic parameters of the system. Slater treated the $BaTiO_3$ perovskite structure as five interpenetrating simple cubic lattices. He assumed that all ions have an electronic polarizability but that only the titanium ion has an ionic polarizability and calculated the local field at each ion position. He then expressed the polarization of each simple cubic lattice in terms of the local field which consists of the applied field and the field at each site due to the polarization of the ions on all the simple cubic lattices. The condition for a spontaneous polarization is then the vanishing of a fifth-order determinant. He solved for

the total polarization of the lattice in terms of the applied field, the electronic polarizabilities of all the ions, and the ionic polarizability of the titanium ion. Using experimental values for the electronic polarizabilities, he found that the polarizability catastrophe would take place if the ionic polarizability of the titanium ion assumed a value of only one-sixteenth of the value predicted in the case of simple cubic symmetry. The perovskite structure therefore serves to enhance the onset of ferroelectricity.

Slater also calculated the Helmholtz free energy for $BaTiO_3$. A general derivation of the free energy is given below and a few comments about the specific case of $BaTiO_3$ follow. We first assume that the potential of a displaced ion is

$$\phi(x,y,z) = a(x^2 + y^2 + z^2) + b_1(x^4 + y^4 + z^4) + \\ + 2b_2(x^2y^2 + y^2z^2 + z^2x^2). \qquad (19)$$

This is not an entirely arbitrary assumption since Slater has shown that a potential function of this form will give a temperature dependence of the polarizability which is consistent with Curie-Weiss behavior. The problem is treated entirely with classical statistical mechanics with the understanding that the results would need corrections at temperatures sufficiently low that the partition function summation can no longer be approximated by an integral. The first step is to compute the partition function, Z. If we were dealing with a single polarizable ion, this would be $(2\pi mkT/h^2)^{3/2}W$, where m is the mass of the ion; T, the temperature; k, Boltzmann's constant; h, Planck's constant and

$$W = \int \exp[-\phi + q\underset{\sim}{E}\cdot\underset{\sim}{r})/kT]dv. \qquad (20)$$

If the system contains N identical ions which vibrate independently of each other, the whole partition function is

$$Z = [(2\pi mkT/h^2)^{3/2}]^N W^N/N! \sim [(e/Nh^3)(2\pi mkT)^{3/2}]^N W^N, \qquad (21)$$

where Stirling's formula has been used for the factorial in the last expression in Eq. 21. Inserting Eq. 19 into Eq. 20, one finds

$$W = \int \exp\{[-a(x^2+y^2+z^2)-b_1(x^4+y^4+z^4)-2b_2(x^2y^2+y^2z^2+z^2x^2) + q(E_x x + E_y y + E_z z)]/kT\}. \qquad (20')$$

This equation cannot be solved exactly, we will therefore use series expansion methods, treating b_1 and b_2 as small quantities, and disregarding all terms of higher powers than the first in these quantities.

Consider the part of the exponential in Eq. 20' which does not depend on b_1 and b_2,

$$\exp\{[-a(x^2+y^2+z^2)+q(E_x x + E_y y + E_z z)]/kT\} =$$

$$\exp(q^2E^2/4akT)\exp\{-\frac{a}{kT}[(x - \frac{qE_x}{2a})^2 + (y - \frac{qE_y}{2a})^2 + (z - \frac{qE_z}{2a})^2]\}. \qquad (22)$$

In Eq. 22, we have completed the square in the exponential and used the relation $E^2 = E_x^2 + E_y^2 + E_z^2$. The other part of the exponential in Eq. 20' can now be expanded in the manner mentioned above. This

expansion gives

$$\exp\{[-b_1(x^4+y^4+z^4)-2b_2(x^2y^2+y^2z^2+z^2x^2)]/kT\} =$$

$$1 - \frac{b_1}{kT}(x^4+y^4+z^4) - \frac{2b_2}{kT}(x^2y^2+y^2z^2+z^2x^2). \qquad (23)$$

Using Eq. 22 and Eq. 23, Eq. 20' becomes

$$W = \exp(q^2E^2/4akT) \int \exp\{-\alpha[(x-Q_x)^2+(y-Q_y)^2+(z-Q_z)^2]\} \cdot$$

$$\cdot[1-\beta_1(x^4+y^4+z^4)-2\beta_2(x^2y^2+y^2z^2+z^2x^2)]dV, \qquad (24)$$

where

$$\alpha \equiv \frac{a}{kT}, \quad \beta_1 \equiv \frac{b_1}{kT}, \quad \beta_2 \equiv \frac{b_2}{kT} \quad \text{and} \quad Q_i = \frac{qE_i}{2a} \quad \text{for } i=x,y,z.$$

There are three types of integrals to be evaluated in Eq. 24:

$$\int_{-\infty}^{\infty} e^{-\alpha(i-Q_i)^2} di = \sqrt{\pi/\alpha}, \qquad (25)$$

$$\int_{-\infty}^{\infty} (i)^4 e^{-\alpha(i-Q_i)^2} di = \sqrt{\pi/\alpha}\,[Q_i^4 + 3Q_i^2(\tfrac{1}{\alpha}) + \tfrac{3}{4}(\tfrac{1}{\alpha})^2], \qquad (26)$$

$$\int_{-\infty}^{\infty} (i)^2 e^{-\alpha(i-Q_i)^2} di = \sqrt{\pi/\alpha}\,[Q_i^2 + \tfrac{1}{2}(\tfrac{1}{\alpha})]. \qquad (27)$$

Using these results, Eq. 24 becomes

$$W = \left(\frac{\pi kT}{a}\right)^{3/2} \exp(q^2E^2/4akT)\{1 - \tfrac{3}{4}(3b_1+2b_2)(kT/a^2)$$

$$- \frac{q^2}{4a^3}(3b_1+2b_2)(E_x^2+E_y^2+E_z^2) - \frac{q^4}{16a^4kT}\,[b_1(E_x^4+E_y^4+E_z^4)$$

$$+ 2b_2(E_x^2E_y^2 + E_y^2E_z^2 + E_z^2E_x^2)]\}. \tag{28}$$

The Helmholtz free energy is given by the following relation:

$$A = -kT \ln Z, \tag{29}$$

where Z is the partition function. Using this and Eqs. 21 and 28, the Helmholtz free energy becomes:

$$A = -NkT \ln[(e/Nh^3)(\pi kT)^3(2m/a)^{3/2}] - N\frac{q^2E^2}{4a}$$

$$+ \frac{3N(kT)^2}{4a^2}(3b_1+2b_2) + \frac{q^2E^2}{4a^3}(3b_1+3b_2)NkT + \frac{Nq^4}{16a^4}[b_1(E_x^4 +$$

$$+ E_y^4+E_z^4) + 2b_2(E_x^2E_y^2 + E_y^2E_z^2 + E_z^2E_x^2)], \tag{30}$$

where the approximation $\ln(1-x) \sim x$ for small x has been used. The free energy used in the previous section was the Gibbs free energy which is defined by the relation

$$G = A + E_xP_x + E_yP_y + E_zP_z, \tag{31}$$

where P_i is the polarization in the i direction and is given by

$$P_i = -\left(\frac{\partial A}{\partial E_i}\right)_T, \qquad i = x,y,z. \tag{32}$$

The polarization can now be calculated from Eq. 30 and the Gibbs

energy determined as a function of P and T:

$$G = -NkT\ \ln[(e/Nh^3)(\pi kT)^3(2m/a)^{3/2}+3N(kT)^2(3b_1+2b_2)/4a^2$$

$$+\frac{aP^2}{Nq^2}\left[1+\frac{kT}{a^2}(3b_1+2b_2)\right]+\frac{1}{N^3q^4}\left[b_1(P_x^4+P_y^4+P_z^4)\right.$$

$$\left.+2b_2(P_x^2P_y^2+P_y^2P_z^2+P_z^2P_x^2)\right]. \qquad (33)$$

To compare this with Eq. 9 of the last section, let $P_y = P_z = 0$ and P_x be nonzero and equal to P. Then,

$$G = -NkT\ \ln[(e/Nh^3)(\pi kT)^3(2m/a)^{3/2}]+\frac{3N(kT)^2}{4a^2}(3b_1+2b_2)$$

$$+\frac{aP^2}{Nq^2}\left[1+\frac{kT}{a^2}(3b_1+2b_2)\right]+\frac{1}{N^3q^4}b_1P^4. \qquad (34)$$

The above approach has two limitations. First, we assumed that the various ions vibrated independently of each other. This assumption is, of course, incorrect. If we consider these interactions between ions, we must introduce normal coordinates describing the various lattice vibrational modes of the crystal. Such a treatment has been considered by Anderson[2] and Cochran[3] and will be mentioned in the next section. For our purpose, in this section, this treatment is not necessary and will not be considered.

The second limitation of the above calculation is that we have not considered the effect of the long-range dipole fields. The ions, by their displacements, produce long-range electric forces acting on each dipole of the system, and these dipole forces must be considered separately from the short-range forces. Slater considered this effect

in detail for the case of $BaTiO_3$ and calculated a Gibbs free energy very similar to Eq. 33, but with additional factors multiplying the last two terms in that equation.

The term in Eq. 34 of interest in the polarization dependent dielectric constant measurements is the coefficient of the fourth-order polarization term. As mentioned in the last section, this coefficient determines the order of the ferroelectric transition. From Eq. 34, this term is b_1/N^3q^4, while Slater calculated a value of $(c_4/\varepsilon_o c_5)^4(Nq^4/16a^4)b_1$, taking into account the dipole fields. In the last expression, c_4 and c_5 are functions of the polarizabilities of the barium and oxygen ions in $BaTiO_3$. The important thing to note about the form found for the fourth-order polarization coefficient is that its sign depends only on the sign of b_1, the coefficient of the anharmonic contribution to the ion potential. For a first-order transition, b_1 must be negative and for a second-order transition, it must be positive. In the case of KTN, b_1 must be a function of composition since it changes from positive to negative at some critical composition.

3. Lattice Dynamics

Anderson[2] and Cochran[3] have investigated the phenomenon of ferroelectricity in terms of the normal modes of vibration. Fröhlich[23] first suggested that these modes might be very important in the theory of ferroelectricity from a consideration of the Lyddane-Sachs-Teller relation (Eq. 4). That is, the high value of the static dielectric constant at the transition is caused by an

unusually low frequency for one of the transverse optical vibrational modes.

Cochran has solved for the transverse optic phonon mode frequency for a diatomic cubic crystal in which each ion is surrounded by tetrahedral symmetry. The calculations are made at zero wave number where the lattices of like atoms are vibrating as a single unit. He used a "shell" model which had proved to be quite successful in describing the dispersion relations of sodium iodide.[24] In this model, each ion is represented as a core, consisting of the nucleus and inner electrons, and a shell representing the outer electrons. The core is coupled to the shell by an isotropic force constant. The forces acting at each lattice site are then the long-range Coulomb forces, which depend on the lattice polarization and act on each core and shell, and the short-range core-core, shell-shell and core-shell interactions. The diatomic lattice can then be considered to consist of four interpenetrating lattices each vibrating as a single unit. Cochran writes the equations of motion for each sublattice, assumes that the shells have zero mass, and solves for the frequency of the transverse optical phonon mode. The square of the mode frequency is proportional to the difference between terms representing the short-range restoring forces and the long-range Coulomb forces. The unusually low value of the mode frequency at the ferroelectric transition, therefore, results from a near cancellation of the short-range and Coulomb interactions.

Cochran next assumes a short-range potential function for the core-core interaction. This potential is of the same form as that

assumed by Slater (Eq. 19). The short-range force is determined from the potential by differentiation and plotted as a function of a general ion displacement, u, in Figs. 2 and 3. The Coulomb force is also shown and is assumed to be linearly temperature dependent. The square of the T.O. mode frequency is now proportional to the difference between the slopes of these two curves at the origin while the dielectric constant is inversely proportional to the same quantity.

Figure 2 shows the forces for three different temperatures in the case where the coefficient of the fourth-order term in the potential, b_1 in Eq. 19, is positive. The condition for a structural transition can be determined by the external mechanical work necessary to cause the transition. In Fig. 2a, the work necessary to displace the ions a distance u_o from equilibrium is equal to the difference between the area under the curve representing the short-range force and the area under the curve representing the Coulomb force. Since this work is positive in Fig. 2a, the stable state of the system is the equilibrium position, $u = 0$. As the temperature decreases, the two curves become tangent at the origin (Fig. 2b), and as the temperature decreases further (Fig. 2c), the amount of work necessary to displace the ions to a new position u_o is negative and this becomes the new equilibrium position of the ions. In this case, the equilibrium displacement is a continuous function of temperature changing from zero at the transition to some positive value. This is then, a second-order transition. Since the dielectric constant is inversely proportional to the difference between the two slopes at the origin, it

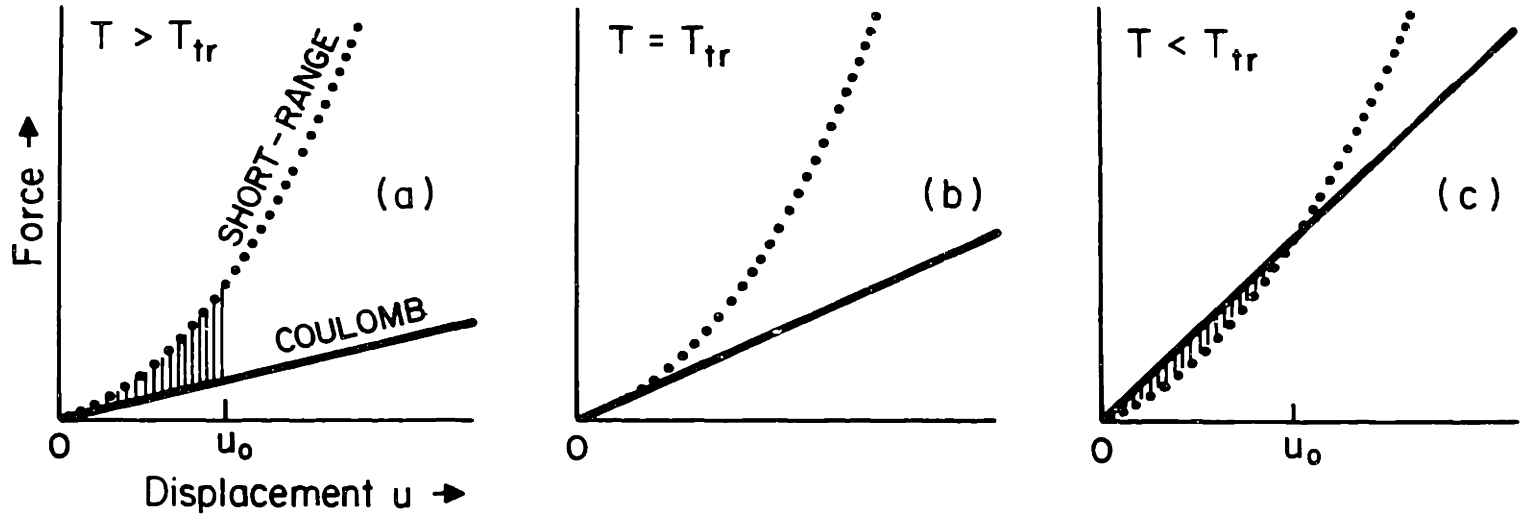

Fig. 2. Short-range and Coulomb forces vs. displacement for $b_1 > 0$.

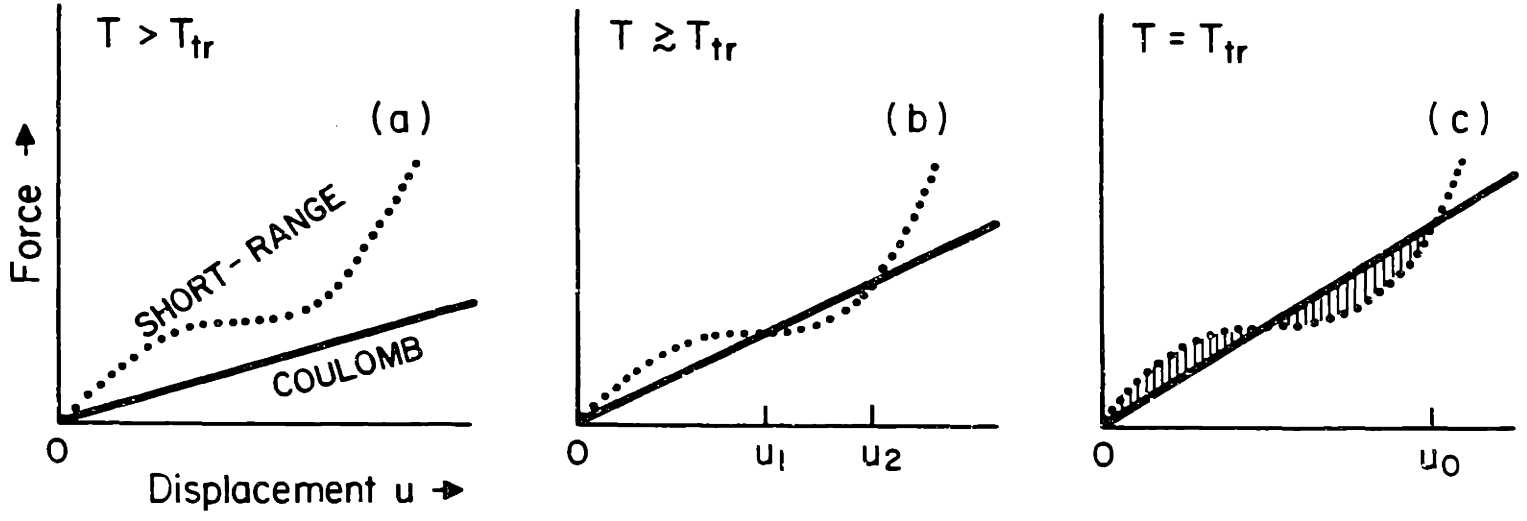

Fig. 3. Short-range and Coulomb forces vs. displacement for $b_1 < 0$.

is infinite at the transition. Also, the T.O. mode frequency is zero at the transition since it is directly proportional to the same quantity.

The conditions for the case in which b_1 is negative in Eq. 19 are shown in Fig. 3 for three different temperatures. The intersections corresponding to u_1 and u_2 are unstable since work is required to displace the ions to these positions. The stable condition for the system in Figs. 3a and 3b is therefore at $u = 0$. As the temperature is lowered, the two shaded areas in Fig. 3c become equal and no work is required to displace the ions to the position u_o. The ions then change to a new equilibrium position u_o discontinuously and a first-order transition takes place. Since the two slopes are not equal at the transition, the dielectric constant is finite and the soft mode frequency is nonzero at a first-order transition.

Using this argument it is then possible to show that for b_1 positive in Eq. 19, the transition will be second-order while for b_1 negative the transition will be first-order. This same conclusion was reached in the previous section but was formulated in a different manner.

The temperature dependence of the soft mode is assumed to be due to anharmonic terms in the lattice potential since it is known that one effect of the anharmonicity of the lattice vibration is to make the effective harmonic force constant temperature dependent.[25] The soft mode should vary as $(\kappa)^{-1/2}$ in the nonpolar phase where κ is the dielectric constant. Since the dielectric constant usually obeys the Curie-Weiss law in this phase, the soft mode should depend on temper-

ature as $(T-T_o)^{1/2}$, where T_o is the Curie-Weiss temperature. In the polar phase, it will vary in a manner similar to the spontaneous polarization. The temperature dependence of this mode in the nonpolar phase has been observed in $SrTiO_3$,[26] $BaTiO_3$,[27] $KTaO_3$,[28,29] and $(Na,K)TaO_3$.[6]

The physical mechanism for the temperature dependence of the dielectric constant in the Cochran theory is essentially the same as in the theory developed by Slater. Also, the dependence of the order of the transition on the sign of the fourth-order coefficient in the ion potential was previously suggested by the Slater model. The main contribution of the Cochran theory is that it correlates the transition to the polar state with the existence of a temperature-dependent transverse optic phonon, thus enabling one to study the ferroelectric behavior with the techniques available for observation of the lattice vibration mode.

4. Raman Effect

In the Raman effect, one observes light inelastically scattered from the system being studied. The frequency spectrum of the observed light can be discussed in completely classical terms. The incident radiation induces dipole moments in the system. For small field intensities, the response of the dipoles to the electric field is linear and

$$\underset{\rightarrow}{M} = \alpha \underset{\rightarrow}{E}, \tag{35}$$

where M is the dipole moment, α is the polarizability, and E is the electric field. The polarizability is, in general, a second-rank tensor and can be represented by an ellipsoid. In Eq. 35 we have

assumed that the three principal axes of the ellipsoid are equal to α. The electric field can be written as a function of time in the following form:

$$\underset{\rightarrow}{E} = \underset{\rightarrow}{E}_m \cos(\omega_i t). \tag{36}$$

Inserting this into Eq. 35, one finds

$$\underset{\rightarrow}{M} = \alpha \underset{\rightarrow}{E}_m \cos(\omega_i t). \tag{37}$$

If it is assumed for the sake of simplicity that all the ions in the crystal vibrate with a frequency ω_p, the polarizability will change with the ion configuration. If the ions execute a periodic motion, α will change in a periodic manner and one may write:

$$\alpha = \alpha_o + \alpha_1 \cos \omega_p t, \tag{38}$$

where α_o is the polarizability in the equilibrium configuration. Substituting Eq. 38 into 37 leads to the expression

$$\underset{\rightarrow}{M} = (\alpha_o + \alpha_1 \cos \omega_p t)(\underset{\rightarrow}{E}_m \cos \omega_i t)$$

$$= \alpha_o \underset{\rightarrow}{E}_m \cos \omega_i t + \frac{\alpha_1}{2} \underset{\rightarrow}{E}_m [\cos(\omega_i - \omega_p)t + \cos(\omega_i + \omega_p)t]. \tag{39}$$

The electric moments induced therefore radiate light which contains three frequency components. The component corresponding to the incident frequency, ω_i, gives rise to the Rayleigh line in the scattering spectrum. The other components, $\omega_i - \omega_p$ and $\omega_i + \omega_p$, correspond to the so-called Stokes and anti-Stokes lines observed in the Raman effect. An important point to notice in this classical treatment is that the Rayleigh scattering results from the polarizability of the ions while the Raman scattering components

result from the change in polarizability.

A quantum mechanical description is necessary to explain the quantization of the vibration modes. In the quantum description, the line at $\omega_i - \omega_p$ (Stokes line) corresponds to a process in which the incident radiation gives energy to the lattice and creates a phonon. In this case, ω_i is the frequency of the incident light and ω_p is the frequency of the phonon. The line at $\omega_i + \omega_p$ (anti-Stokes line) corresponds to the process in which the incident radiation receives energy from a lattice vibrational mode and thus annihilates the phonon. The probability of the anti-Stokes process is proportional to the number of thermally excited phonons, $\bar{n}$, where $\bar{n}$ is the Bose factor,

$$\bar{n} = [\exp(\hbar\omega/kT)-1]^{-1}.$$

The probability of the Stokes process can be shown to be proportional to $(\bar{n} + 1)$. Therefore, the intensity of the Stokes component in the scattering spectrum is greater than that of the anti-Stokes component.

For processes in which a single phonon is created or destroyed, the phonon wave vector is determined by the wave vector of the incident and observed light. Conservation of momentum and energy require that

$$\vec{k}_i + \vec{k}_o + \vec{k}_p = 0 \quad \text{and} \quad \omega_i = \omega_o \pm \omega_p,$$

where $\vec{k}_i$, $\vec{k}_o$, and $\vec{k}_p$ are the wave vectors of the incident light, observed light, and the phonon. ω_i, ω_o, and ω_p are the respective frequencies. For incident light in the visible spectrum, and for incident and observed light at right angles, a phonon wave vector has a magnitude of order 10^5 cm^{-1}, which is smaller than a typical Brillouin zone by

about a factor 10^3. The first-order scattering therefore corresponds to annihilation or creation of a phonon with wavelength very large compared to a lattice constant.

Higher order Raman processes can also be observed in which two or more phonons are created or annihilated. In this case, the conservation of momentum simply requires that the vector sum of the wave vectors of the incident light, the observed light, and all the phonons involved in the process be zero. One then observes phonon creation and annihilation processes which extend throughout the entire Brillouin zone. The resulting scattering spectrum is therefore a continum. The first-order Raman process is not allowed for crystals in which every ion is at a center of inversion symmetry. This is the case for KTN in its cubic perovskite phase above the paraelectric-to-ferroelectric transition. The "soft" mode is therefore not observable in the nonpolar phase but is observable below the transition since the crystal symmetry changes.

The line shape of the soft modes observed in previous work have varied from relatively narrow modes in $SrTiO_3$[26] and $KTaO_3$ to heavily overdamped modes in $BaTiO_3$[5] and KDP.[30] In the mixed crystal system $(Na,K)TaO_3$,[6] the mode widths were found to vary considerably with composition. For the narrow modes, the mode frequency is simply the peak of the response. In case of overdamping, the modes were assumed to be damped in the same manner as a classical harmonic oscillator, and the undamped frequencies were extracted by fitting the response curves with damped harmonic oscillator functions. In

the case of $(Na,K)TaO_3$, the modes could not be fit by the damped harmonic oscillator functions and a more complicated equation was necessary to fit the line shape.

III. EXPERIMENTAL TECHNIQUES

1. Polarization Dependence of the Dielectric Constant

A technique for measuring the polarization dependence of the dielectric constant has been described by Landauer, Drougard and Young.[31] The technique consists of applying to a capacitance bridge a small high-frequency measuring voltage superimposed upon a large low-frequency sine wave bias field. The bias field polarizes the lattice and the bridge measures the resulting dielectric constant. This method proved unsatisfactory for KTN due to excessive heating of the sample caused by the bias field. To overcome this problem, another technique was employed using a low duty factor (2%) square pulse with zero dc average as the ac bias, Fig. 4a. This bias pulse is generated by the equipment shown in the block diagram in Fig. 5. The pulse repetition is established by an astable multivibrator which generates trigger pulses at 5 hertz. These pulses trigger a Tektronix No. 162 waveform generator, which generates gate waveforms for two Tektronix No. 163 pulse generators. The output of the first generator is a positive going square pulse of 2 msec duration. The output of the second pulse generator is a negative going square pulse of 2 msec duration and delayed 2 msec with respect to the positive going pulse. These two pulses are adjusted to have the same amplitude, and summed in a resistive network. The sum voltage is then amplified by a high-quality 40-watt audio amplifier. The amplifier output drives the 8-ohm secondary winding of a 30 watt high-fidelity audio transformer. The output of the 8000-ohm winding is capacitively loaded to prevent spiking, and applied to the capacitance bridge. The resulting pulse

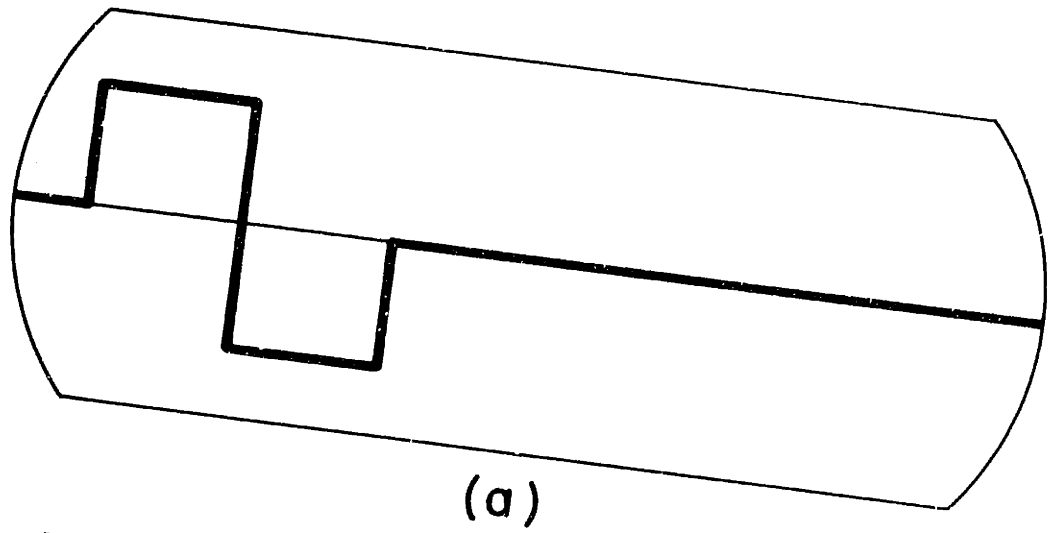

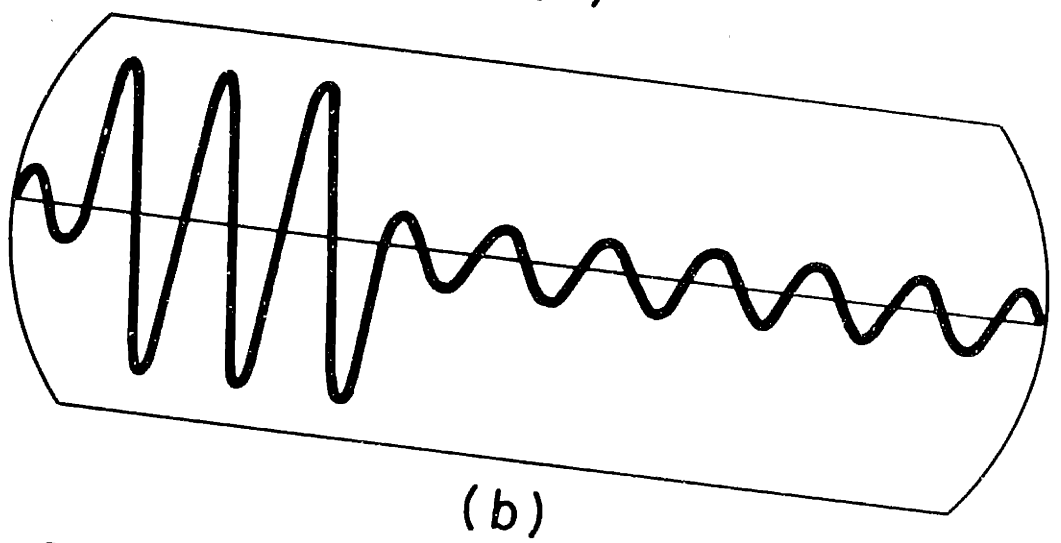

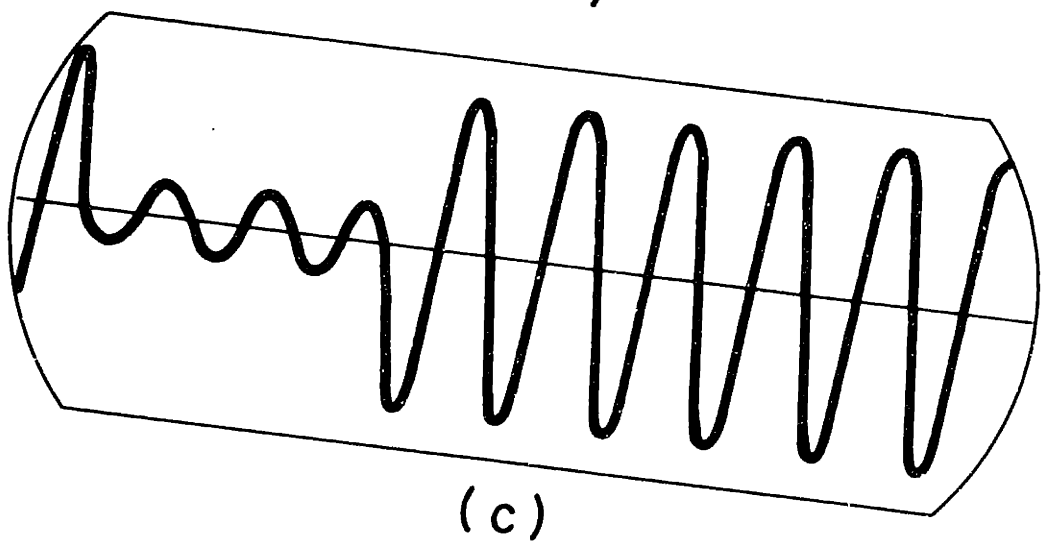

Fig. 4. Oscilloscope traces for polarization dependence measurements.

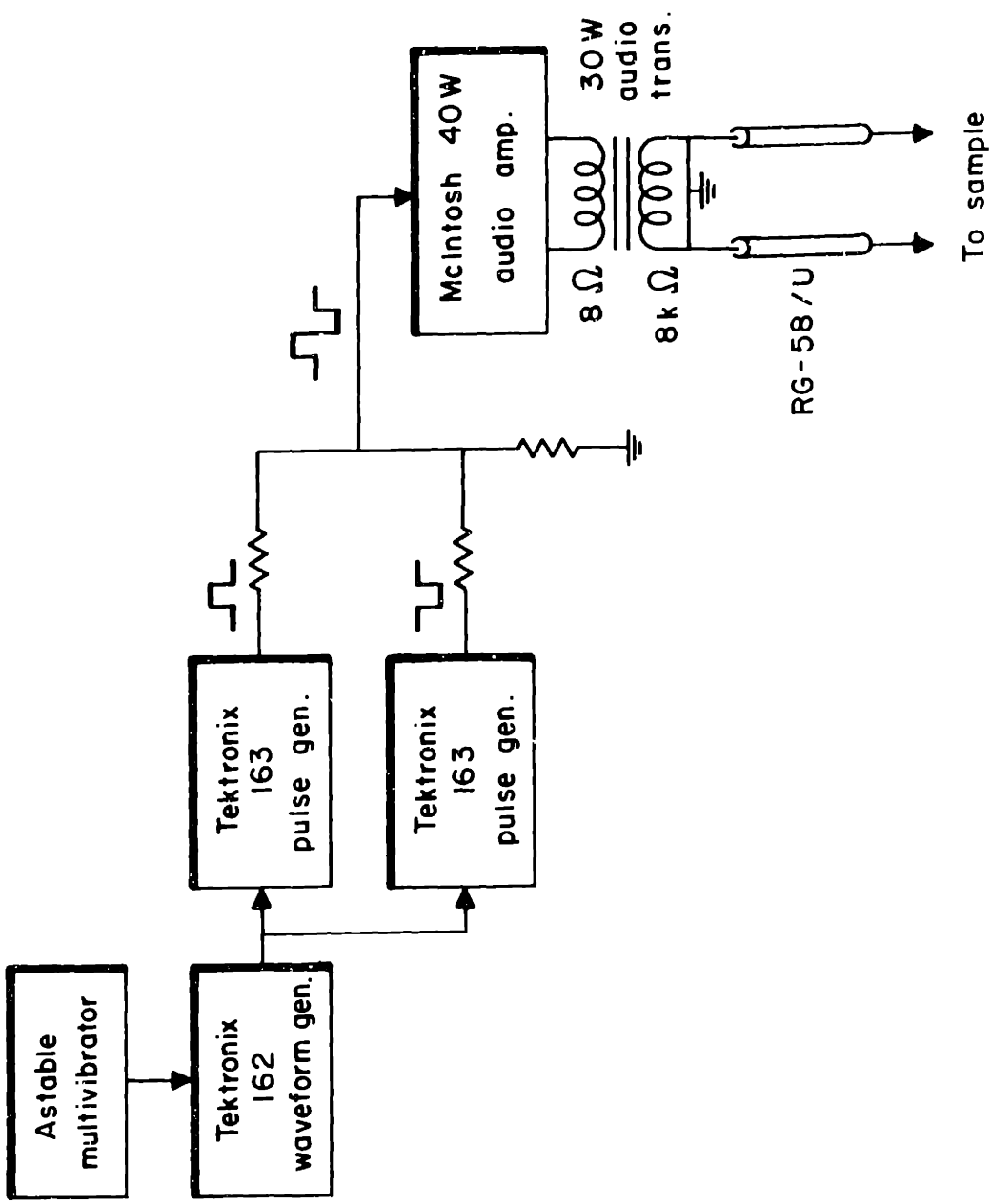

Fig. 5 Equipment for AC bias pulse generation.

has zero DC component, occurs at 10 hertz with a 2 percent duty factor and has a peak amplitude of 0 to 160 volts.

The arrangement for measuring the polarization dependence of the dielectric constant is shown in Fig. 6. The square pulse and a 100-kHz measuring field are applied to the detector terminals of a General Radio 716-C capacitance bridge. The bridge measures the capacitance of the series combination of the sample and a large high-quality linear capacitor. The charge on the linear capacitor is proportional to the polarization of the sample. The bridge unbalance signal is amplified by an amplifier tuned to the measuring frequency, 100 kHz. This amplified bridge signal is then displayed on the oscilloscope (Figs. 4b and 4c) along with the voltage across the linear capacitor (Fig. 4a). In operation, a bias voltage is applied to the bridge, the voltage across the linear capacitor is determined from the oscilloscope trace and the sample polarization computed. The bridge is then balanced for the period in which the pulse is present (Fig. 4c). This bridge reading gives the value of the sample capacitance for the particular value of sample polarization. From these measurements, a plot of $1/\epsilon$ versus P^2 can be constructed and the value of the fourth-order polarization coefficient, B in Eq. 9, determined.

An AC bias is used in the above technique to avoid the difficulty of a space-charge capacitance at the ferroelectric-electrode interface which is usually encountered when a DC bias is used.[32,33] This space-charge capacitance would decrease as the electric field

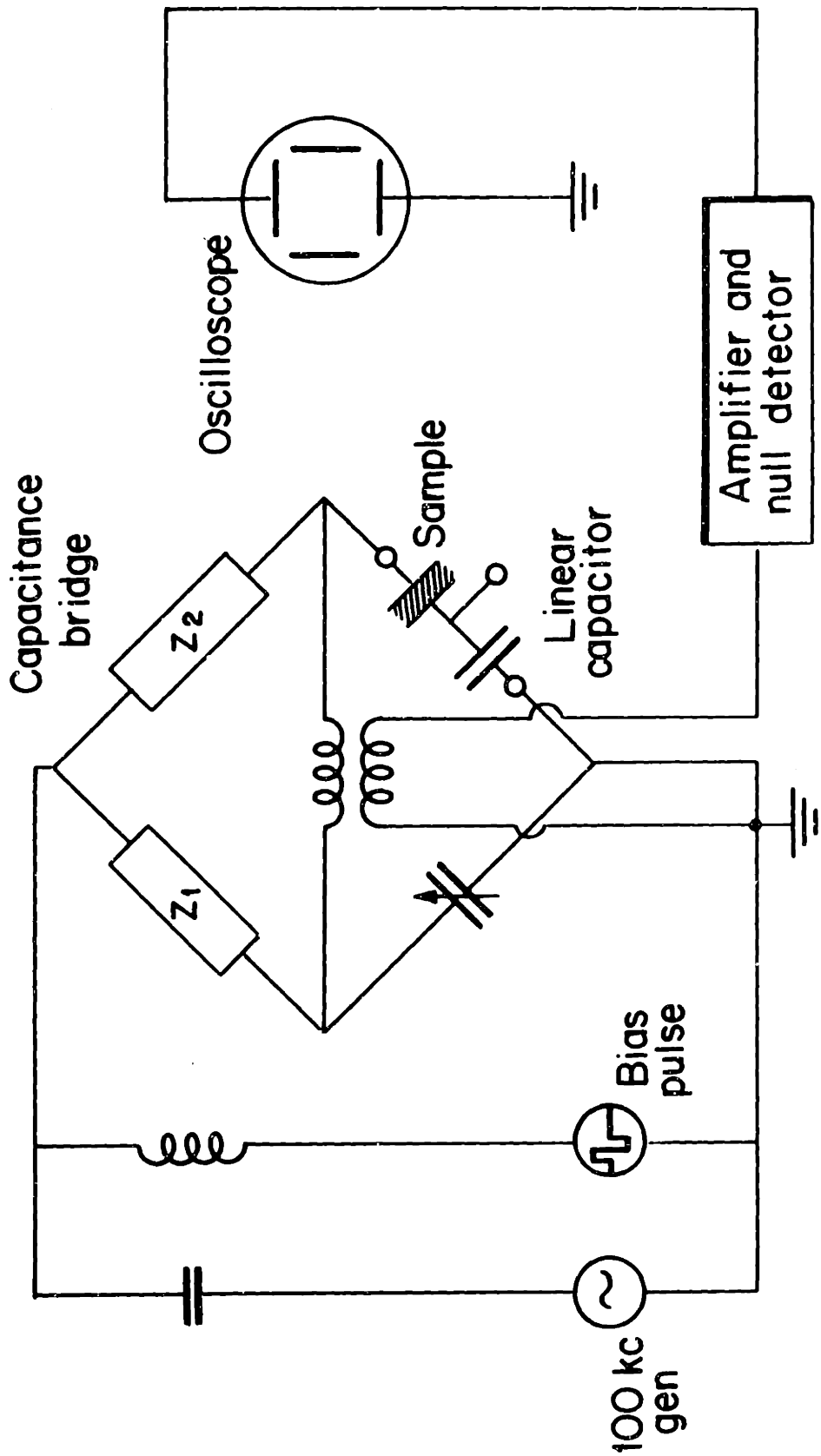

Fig. 6. Experimental apparatus for measurement of $1/\varepsilon$ vs. p^2.

increased and would tend to reduce the field in the bulk of the sample. A slight difficulty with the AC bias technique has been pointed out by Merz.[34] The expression for $1/\epsilon$ in Eq. 11 assumes isothermal conditions while the application of an AC bias is closer to an adiabatic condition. The temperature therefore varies as a function of the polarization. If the temperature increment due to this electrocaloric effect, $\Delta T = T - T_o$, is small, the electric field can be written as

$$E(P,T) = \left(\frac{\partial G}{\partial P}\right)_T = \left(\frac{\partial G}{\partial P}\right)_{T_o} + \left(\frac{\partial^2 G}{\partial P \partial T}\right)_{T_o} \Delta T, \tag{40}$$

where T_o is the temperature at zero polarization. Since the conditions are adiabatic,

$$dS = d\left(-\frac{\partial G}{\partial T}\right) = \left(\frac{\partial S_o}{\partial T}\right) dT - [2\frac{dA}{dT}P + 4\frac{dB}{dT}P^3 + 6\frac{dC}{dT}P^5]dP = 0, \tag{41}$$

where S_o is the entropy of the unpolarized state and where we neglected terms of order P^8 in the free energy. Noting that $\left(\frac{\partial S_o}{\partial T}\right)_{T_o} = \frac{\rho C_p}{T_o}$ and integrating Eq. 41, we get

$$\Delta T = \frac{T_o}{C_p \rho}\left[\frac{dA}{dT}P^2 + \frac{dB}{dT}P^4 + \frac{dC}{dT}P^6\right], \tag{42}$$

where C_p is the specific heat at constant polarization and ρ is the density. Substituting this into Eq. 40, and differentiating, we find

$$\left(\frac{\partial E}{\partial P}\right)_s = \frac{1}{\epsilon - \epsilon_o} \sim \frac{1}{\epsilon} = 2A + 12\left[B + \frac{T_o}{2C_p\rho}\left(\frac{dA}{dT}\right)^2\right]P^2 + 30\left[C + \frac{T_o}{C_p\rho}\left(\frac{dA}{dT}\right)\left(\frac{dB}{dT}\right)\right]P^4. \tag{43}$$

Comparing this with Eq. 11, the correction term to B is found to be

$$B_{correction} = \frac{T_o}{2C_p\rho} \left(\frac{dA}{dT}\right)^2. \tag{44}$$

For KTN, with a composition of 20 mole % $KNbO_3$, the terms in Eq. 44 are listed below. Since both c.g.s. and m.k.s. units are common in the literature, two values are listed for each term, the first being the c.g.s. value. The m.k.s. system is used throughout the present work.

$T_o = 172^oK$

$\rho = 6.5\ g/cm^3 = 6.5x10^3\ kg/m^3$

$C_p = 0.10\ cal/g\cdot degree = 4.18x10^2\ joules/kg\cdot degree$

$\frac{dA}{dT} = 6.29x10^{-5}\ /\ (degree) = 5.65x10^5\ m/farad\cdot degree$

where the value of ρ was taken from data by Reisman and Banks[35] and the specific heat was assumed to be not less than 0.10 cal/g·degree. These values give a maximum correction term

$$B_{correction} = 0.1x10^8\ joule\ m^5/coul^4.$$

The correction is about seven percent of the value of B measured at this composition. For most compositions studied, the correction was much smaller. In all cases, this can be neglected since the value of B cannot be measured to this accuracy. There is a maximum error of approximately 2% in the value of the polarization determined from experiment and the capacitance can be measured to an accuracy of 0.1%. These errors cause a maximum error in B of about 10%.

The major advantage of this low duty factor AC bias technique is that it eliminates most of the heating problems associated with KTN. Any heating which occurs can be easily noticed by observing the bridge unbalance signal with the bridge balanced for a null in the region in which no pulse is applied (Fig. 4b). Since these measurements are made in the paraelectric phase, heating will cause the sample capacitance to decrease and this region will become unbalanced as the pulse voltage is increased. The bridge will balance at a lower capacitance immediately after the pulse and at a higher capacitance just prior to the beginning of the next pulse indicating that the sample has cooled off in the time between pulses. If the region between pulses remains balanced upon increasing the pulse amplitude, however, the heating is negligible.

In order to see if the low-duty factor pulse technique gave results consistent with the method described by Landauer, Drougard and Young,[31] the fourth-order polarization coefficient for a sample in the $(K,Na)TaO_3$ system was measured using both methods. $(K,Na)TaO_3$, unlike KTN, is not heated by the bias field in the LDY method. The values of B measured by both methods were in good agreement.

A single-polarity pulse was initially used in the polarization dependence measurements. This was found to be unsatisfactory since applying a single-polarity pulse to a nonlinear dielectric causes the base line to shift an amount depending upon dielectric nonlinearities, pulse height, and duty factor. This shift in the base line will cause a DC drop across the linear capacitor and thus cause errors in the calculation of the sample polarization. For this reason,

the above technique, employing a bias pulse which is symmetric with respect to the zero-voltage axis, was used. A problem encountered in this technique was that the capacitance bridge did not null at the same value for each pulse. It was found that by introducing a small copper plate between the spring leaf contact and the sample (see Fig. 7), one could cause the two pulses to null at approximately the same value. It may be that the difference in the two pulses was initially due to a pressure gradient caused by the point contact of the leaf spring and that the copper plate relieved this pressure. The polarization dependence measurements were made with this copper plate in place and the change in the capacitance caused by each pulse differed by at most 3%.

2. Temperature Control

In measuring the polarization dependence of the dielectric constant, it is necessary to measure the change in the sample capacitance due only to changes in the polarization. Any small fluctuation in the temperature will cause the sample capacitance to change since the dielectric constant is strongly temperature dependent near the ferroelectric transition where the measurements are made. A change in the temperature of one degree can result in a change of the dielectric constant by as much as fifteen percent. For this reason, it is necessary to control temperature closely. The measurements were made with a Janis Research exchange gas type Dewar. Thermal contact between the sample is determined by equilibrium between the power dissipated in a heater wound around the top of the sample block, and the cooling

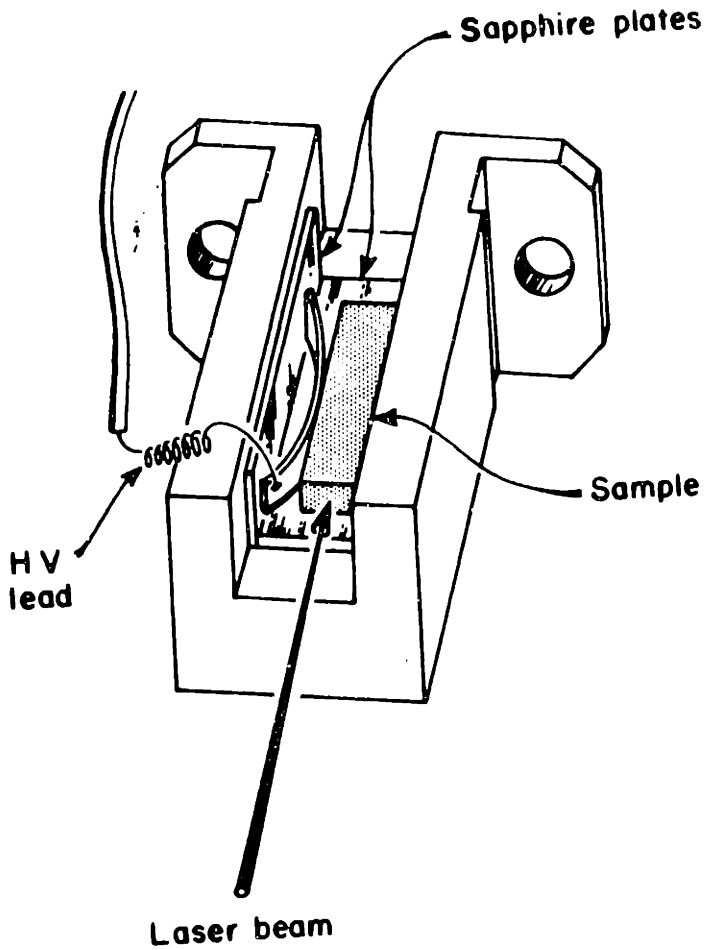

Fig. 7. Sample holder.

rate established by the pressure of the exchange gas. In operation, the exchange gas column is filled with an atmosphere of helium gas and the helium reservoir filled. Then, as the sample approaches the desired temperature, the exchange gas column is pumped down to operating pressure.

The sample block temperature is stabilized by a Princeton Applied Research Model 152 cryogenic temperature controller. The first stage of the controller is a differential amplifier which amplifies the difference between the voltage across a gallium arsenide sensor and the set point voltage. The amplified error signal is then applied to a second stage which contains circuitry for the proportional, derivative and integral control functions. The output of this stage drives a power amplifier which powers the heater on the sample block.

The control element for the temperature controller is an uncalibrated gallium arsenide sensor. Two additional temperature sensors were used to determine the temperature of the sample. For temperatures between liquid helium and 45°K, a doped germanium sensor was used. For temperatures above 45°K, a platinum resistance thermometer was used. The resistance of these devices was measured with an AC bridge operating at 100 hertz. The resistances could be determined to the nearest one-half of an ohm, which corresponds to approximately 0.3°K. The stability of the controller is about 0.1°K.

Using an exchange gas pressure of one atmosphere, and no heater power, the minimum temperature which could be obtained was about 6.5°K. During the experiments, temperatures between 6.5°K and room

temperature were used with indicated exchange gas pressures between 2 and 50 microns, and maximum heater power of about 0.1 watt.

In the course of the polarization dependence measurements, temperature fluctuations could be easily noticed as an overall increase in the bridge unbalance signal since the capacitance is quite sensitive to temperature changes. For the data reported, capacitance fluctuations of less than 0.5 percent occurred during the measurements.

3. Sample Holder

The sample holder used for both the dielectric and scattering measurements is shown in Fig. 7, with a sample and high-voltage contact in place. The holder is constructed from oxygen-free copper to minimize thermal gradients. The sample sits in a square well which extends the length of the holder. For the scattering measurements, the only field applied was the high-frequency measuring field used to measure the sample capacitance. In that case, the ground for the high voltage lead was connected to the Dewar body and one of the electroded faces of the sample was pressed against the side of the sample well. The sample is insulated from the back of the well by a sapphire plate to insure maximum thermal contact and electrical isolation. The brass leaf spring which forms the high-voltage electrode is pressed between the sample and another sapphire plate which insulates the spring from the other side of the square well.

It was necessary to isolate the sample from ground in the polarization dependence measurements. A linear capacitor was placed

between the sample and ground, and the voltage across the capacitor was read from an oscilloscope. The other alternative was to place the linear capacitor in the high-voltage lead and read the voltage from the scope using the differential mode which is limited in sensitivity to 1 volt/cm. This was inadequate since the linear capacitor voltage varies only from zero to one volt during the course of each experiment. For these measurements, then, another electrode was epoxied to a sapphire plate and placed between the sample and the right-hand side of the sample well in Fig. 7.

The two temperature sensors are set into holes in the copper block just behind the sample. They were coated with high thermal conductivity paste and pressed into place. The gallium arsenide control element is located in a hole directly behind the sample well near the top of the sample block and is held in place with indium solder.

4. Optical and Detection Systems

The excitation source for the Raman scattering experiment was an argon laser with power output of 150 to 200 milliwatts in the 4880 Å line. The general geometrical arrangement of the scattering experiment is shown in Fig. 8. The laser beam is refracted in two high-index spectrometer prisms to separate the 4880 Å line from the nonlasing light in the argon discharge. Two slits are located in the optical path to block this nonlasing light and keep it from entering the sample. The beam is deflected vertically into a 5 cm focal length microscope objective, which brings the light to a focus in the sample. The microscope objective is mounted on a carriage which permits micro-

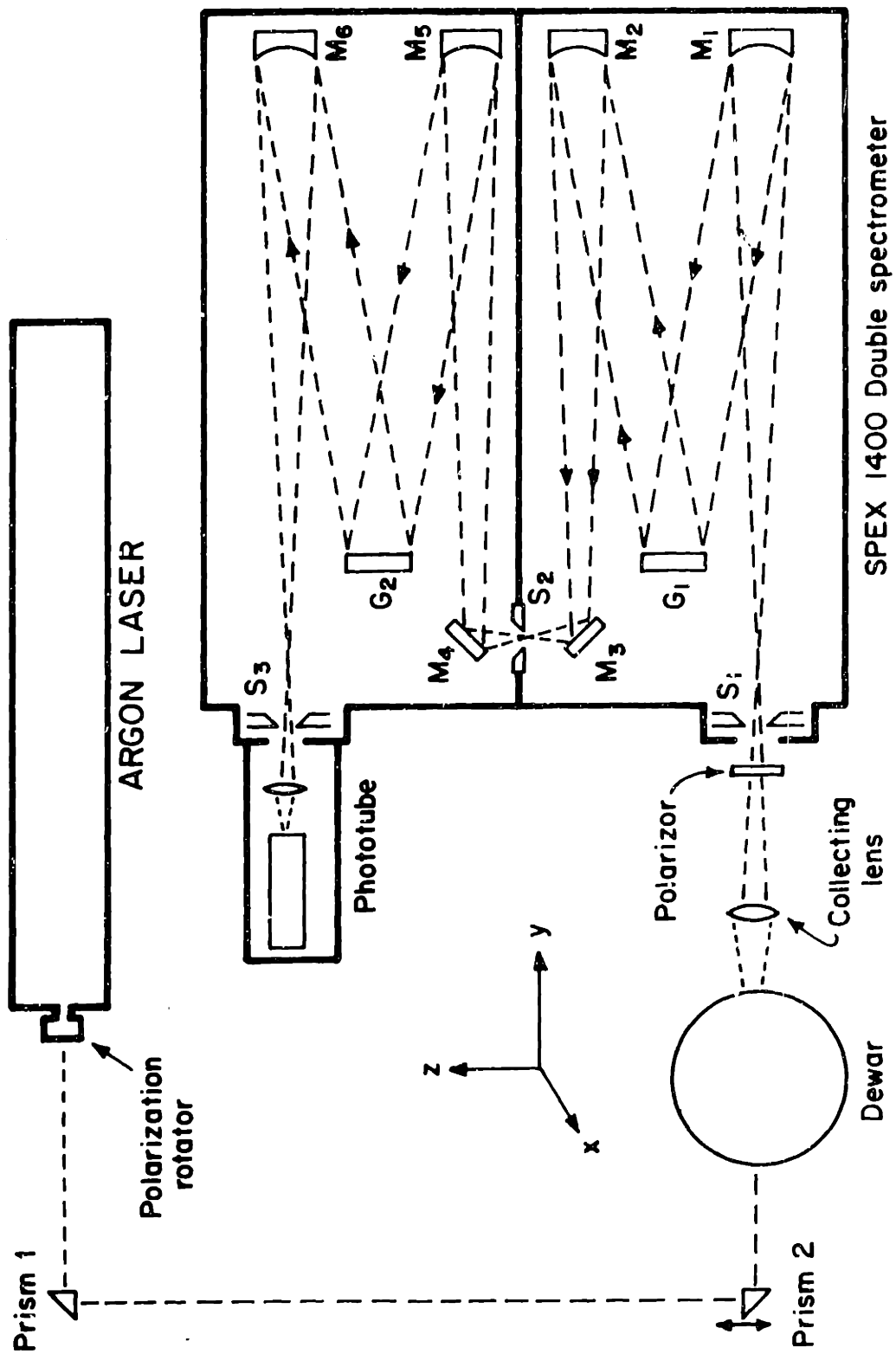

Fig. 8. Optical diagram of scattering experiment.

meter adjustments of the three translational degrees of freedom. Also, the Dewar mount allows small adjustments in the Dewar position in the x,y,z directions. This arrangement allows very precise positioning of the beam in the sample. The scattered light is observed at a right angle with respect to the laser beam and is collected by a Tektronix Fl. 9 camera lens. This lens is also mounted to allow micrometer adjustments of the three translational degrees of freedom. It is positioned so that the sample image slightly overfills the entrance slit of the spectrometer.

The spectrometer used in the experiment was a Spex 1400 double grating spectrometer, shown schematically in Fig. 8. It consists of two identical 3/4-meter Czerny-Turner spectrometers side by side. The exit slit of the first is the entrance slit of the second. The gratings are driven by the same lead screw. Both gratings were 1200 lines/mm, blazed at 5000 angstroms. It is necessary to use a double spectrometer since the Raman modes observed occurred within one-hundred wave numbers of the Rayleigh line. It is therefore essential that the exciting line be rapidly attenuated. For a single spectrometer, the signal due to the Rayleigh line is attenuated with displacement from the exciting wavelength reaching a value of 10^{-5} or 10^{-6} times the light incident on the grating. Many of the Raman signals are smaller than this and are therefore masked by the stray light. For a double spectrometer, the attenuation of the Rayleigh line is much more rapid, the stray light eventually reaching levels of 10^{-10} or 10^{-12} times the light incident on the first grating.

Since the Raman modes have frequencies of only a few wave numbers

near the transition, it is desirable to make observations as close to the exciting line as possible. To do this, an arrangement was constructed with an optical attenuator affixed to the shaft of a solenoid. When the solenoid is activated, the attenuator moves into the optical path and attenuates the laser line by a factor of about 10^4. This allows the laser line to be scanned without any damage to the phototube. As soon as the scattered radiation reaches a tolerable level, the solenoid is deactivated and the attenuator is removed from the optical path. This arrangement allows scattering to be observed only 2 cm^{-1} from the laser line and also allows one to determine the location of the excitation line with respect to the calibration marks provided by the spectrometer.

The Raman lines observed were found to have widths of several angstroms. A spectrometer resolution of .5 to 1 angstrom was, therefore, considered adequate in most cases. In some instances, mode splittings of 1 $\mathring{A}$ were resolved with all three spectrometer slits at 40 microns and slit height 5 mm. This setting was used for almost all scattering measurements.

The detection system is a photon counting system. The output flux is detected by an FW-130 phototube. The phototube signal is amplified and the resulting pulses are counted in a Hewlett Packard 5280A Counter. The counting period is determined by external gating circuitry and was set to be two seconds in most cases. The output of the counter then goes to a Hewlett Packard 581A digital-to-analog converter and the output of the converter is plotted on a strip chart

recorder. The dark count of the phototube was typically 200 counts per second, while all mode signals were at least 3000 counts per second. It was therefore not necessary to cool the phototube.

As was mentioned in the Raman scattering section, first-order Raman scattering is not allowed in the cubic nonpolar phase. A technique for relaxing this selection rule, and making the soft mode Raman-active in the cubic phase has been described by Fleury and Worlock.[36] The method consists of applying an AC field to the sample along one of the cubic axes, thus changing the symmetry of the lattice. The scattered radiation is then synchronously detected in a box-car integrator. The scattered radiation synchronous with the applied field then corresponds to scattering by processes which are forbidden in the cubic phase. Field induced scattering in the nonpolar phase was observed in some crystals but, due to experimental difficulties, most scattering was observed in the polar phases.

5. Crystal Growth and Sample Preparation

The KTN crystals were grown by the technique described by Wemple[19] for $KTaO_3$. The method is a top-seeded solution growth from a melt consisting of Ta_2O_5 and K_2CO_3. The melt, contained in a platinum crucible, is heated to approximately 1400°K. Upon heating, the K_2CO_3 decomposes into K_2O and CO_2 leaving K_2O and Ta_2O_5 in the melt. The temperature is lowered at a rate of approximately one-half of a degree per hour and growth begins to take place at about 1370°K. The crystal is pulled from the melt during the growth process at a rate of one-half of a millimeter per hour. The growth of KTN is similar to this but with Nb_2O_5 substituted

for part of the Ta_2O_5. The growth temperature depends on the melt composition and varies from 1372°K for $KTaO_3$ to 1064°K for $KNbO_3$. The phase diagram for the KTN system has been determined by Reisman, Triebwasser, and Holtzberg.[37] In the present study, the first KTN crystal was grown with low niobium concentration using pure $KTaO_3$ as the seed. Seeds from the resulting crystal were then used for the growth of the next higher concentration, etc. Crystals were grown in the composition range 5 to 60 mole % $KNbO_3$. They were typically of 1 to 3 cm^3 volume with well developed (100) faces. The crystal composition was determined by the volumetric method of Headridge and Taylor.[38] Then, knowing the composition of the melt, a plot of the crystal composition versus melt composition could be constructed. These results are shown in Fig. 9, and a description of the volumetric method is in the Appendix.

Samples cut from a bulk crystal contained large inhomogeneities in their composition. Samples cut from the top and bottom of a crystal, approximately one centimeter apart, were found to differ in composition by as much as eight mole % $KNbO_3$. It was found, however, that there was excellent homogeneity in the planes perpendicular to the growth direction. Therefore, to minimize inhomogeneities, samples were taken from thin plates cut perpendicular to the growth direction. These sample plates were typically 1 cm^2 in area and 2 mm thick.

The requirements for the scattering and dielectric samples were quite different. The scattering sample had to be about 2 mm thick so that the laser beam could be easily positioned in the sample. The dielectric sample, however, had to be very thin compared to the scattering

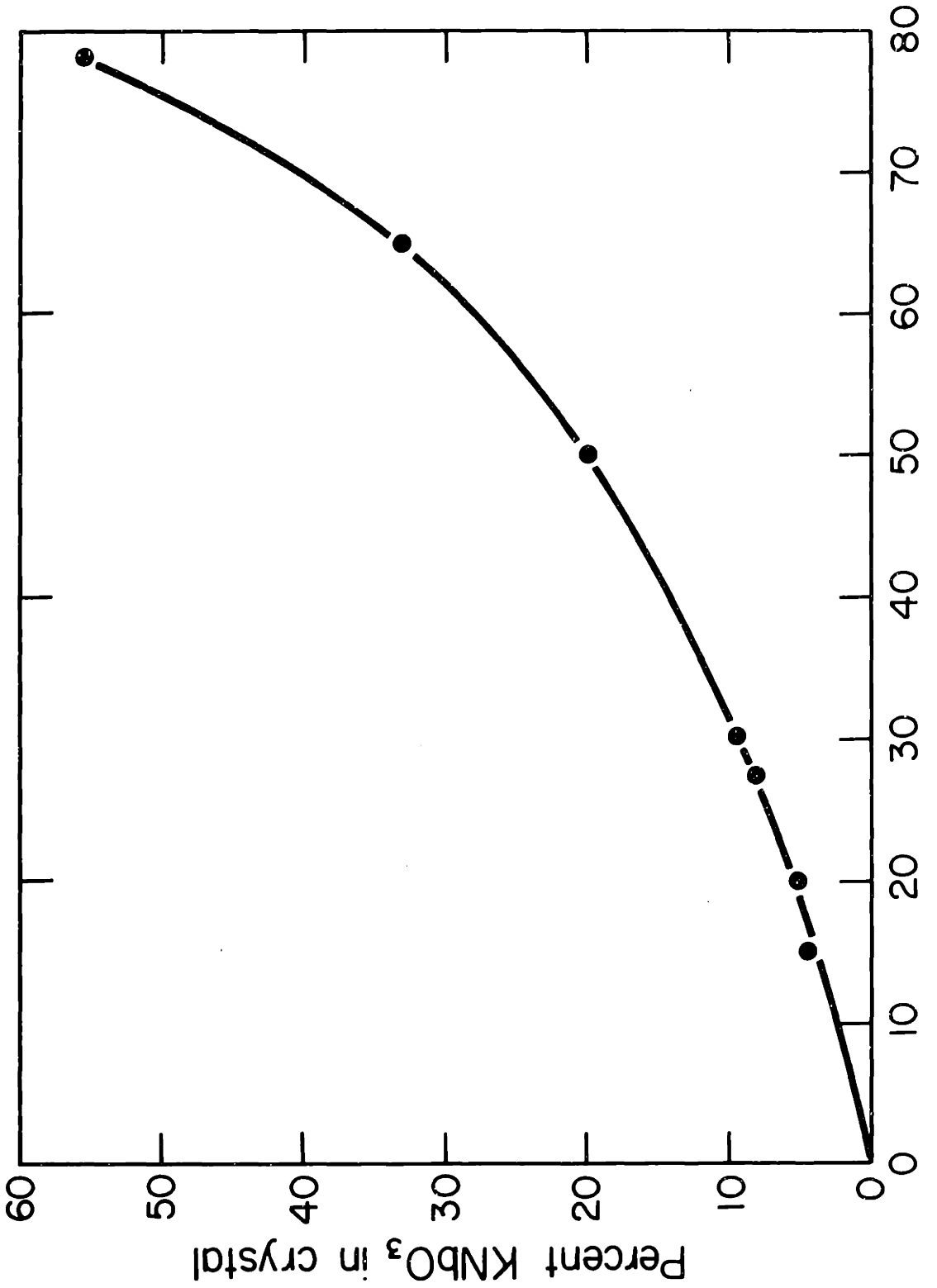

Fig. 9. Crystal composition vs. melt composition for KTN.

sample so that large fields could be applied to measure the polarization dependence of the dielectric constant and also to minimize the inhomogeneities in the sample. It was therefore necessary to cut two samples from each sample plate. The sample plates were observed between crossed polarizers before the samples were cut. The observations usually revealed areas of large strain and also grain boundaries which divided the sample plate into four regions. The dielectric and scattering samples were always cut from the same region, taking care to avoid intersections with the grain boundaries and the areas of strain.

It was desired to have scattering and dielectric data from the same crystal composition. Therefore, before the sample plate was cut, either the top or the bottom of the plate was chosen as the desired composition and marked. The two samples were then cut from the sample plate. The marked face of the scattering sample was optically polished while the opposite face of the dielectric sample was ground with A.O. compound No. 600 to within 0.4 mm of the marked face. In the scattering experiment, the laser beam is positioned just behind the optically polished face of the scattering sample. This insures that the composition of the scattering region is the same as the composition of the dielectric sample.

The dielectric samples were thinned by polishing with A.O. compound No. 305 to approximately 0.3 mm. The area of the sample faces was typically 6 mm^2. The samples were then cleaned in acetone and alcohol and titanium electrodes were evaporated on the two large faces. The sides of the sample were masked from the evaporation by thin glass

plates, approximately the same thickness as the sample. To protect the titanium from oxidation, a layer of gold was evaporated over it before the vacuum was broken.

The Raman scattering samples were typically 2 mm x 2 mm x 6 mm. Since it is necessary that the scattering take place in a single composition, the laser beam must be in the plane of homogeneity perpendicular to the growth direction. Therefore, the two faces of the sample perpendicular to the growth direction were optically polished. One of these faces coincides with the composition of the dielectric sample as mentioned above. The two ends (2 mm x 2 mm) of the sample were also optically polished since the laser beam enters and exits through these two surfaces. The optical polish was achieved by first polishing the sample with A.O. compound No. 305 to make the surfaces flat and parallel and then polishing with Linde A for the optical finish. The remaining two faces were polished with A.O. compound No. 305 and electroded with titanium and gold so that capacitance measurements could be made during the course of the scattering experiment. In many cases, it was possible to cut the samples such that two or more of the optical surfaces coincided with the natural faces of the bulk crystal, thus eliminating most of the optical polishing.

6. Determination of Crystal Composition

Triebwasser[7] found that the Curie temperature decreased almost linearly with decreasing $KNbO_3$ concentration in the interval 20 to 100 mole % $KNbO_3$, thus providing a convenient means of determining the crystal composition. He did not take any data points in the region

0 to 20 mole % $KNbO_3$, a region of interest in this work. Therefore it was necessary to determine the dependence of the Curie temperature on composition in the range of interest, 0 to 40 mole % $KNbO_3$. For this determination, thin plates were cut from the crystals perpendicular to the growth direction so that the inhomogeneities could be minimized. These plates were cut into two pieces, one for dielectric measurements and the other for chemical analysis. The dielectric samples were thinned by polishing with A.O. compound No. 305 to approximately 0.3 mm and electroded with an indium gallium alloy. The transition temperatures were then determined by measuring the dielectric constant and noting the temperature at which the peaks in the dielectric constant occurred. The other half of the sample was chemically analyzed to determine the sample composition. An accuracy and precision of about $\pm$0.5% was obtained in the composition determination.

The graph of the transition temperatures versus crystal composition is shown in Fig. 10. The three lines correspond to the three transitions in KTN. The transition temperatures become closer together as the $KNbO_3$ concentration is decreased until, at about 5 mole % $KNbO_3$, there is only one transition observed. Below this composition, the exact nature of the structural change is not known. The data appears to extrapolate to a transition temperature of zero or a few degrees below for $KTaO_3$. This is consistent with Wemple's finding that $KTaO_3$ does not undergo a transition to a ferroelectric phase at any attainable temperature. Data points taken in the composition range 20 to 60 mole % $KNbO_3$ agreed quite well with Triebwasser's results.

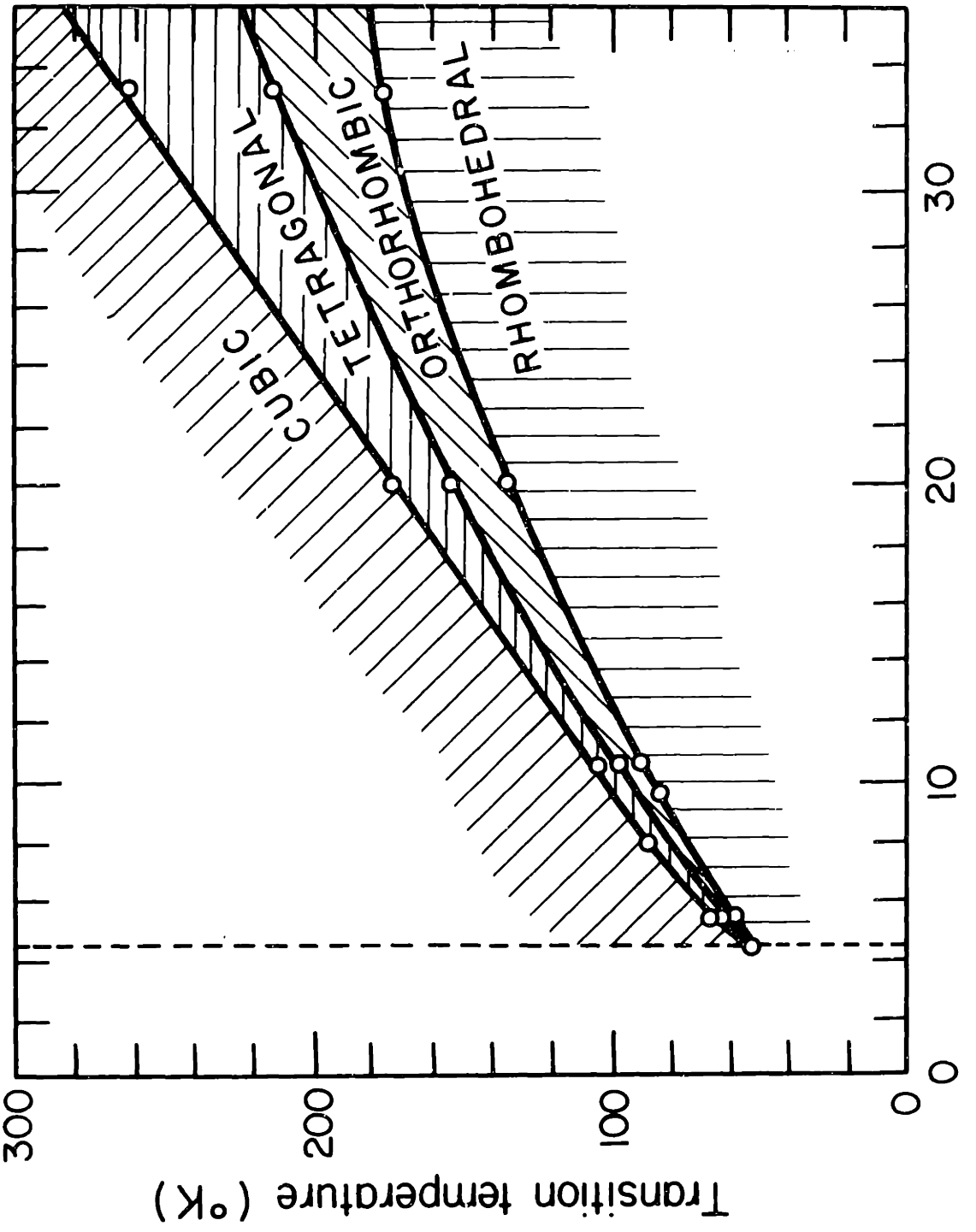

Fig. 10. Transition temperatures vs. crystal composition.

IV. EXPERIMENTAL RESULTS AND DISCUSSION

1. Polarization Dependence of the Dielectric Constant

The polarization dependence of the dielectric constant of five samples was measured. These samples contained 8.0, 19.4, 27.4, 33.2 and 38.8 mole % $KNbO_3$. The polarization dependence of the 19.4 mole % $KNbO_3$ sample is shown in Fig. 11. This plot is quite linear with very little scatter indicating that the sixth and higher order terms are negligible in the free energy and that the polarization dependence of the dielectric constant can be written as Eq. 18. This data was taken at 240°K, 16°K above the paraelectric-to-ferroelectric transition, and gives a value of B equal to 3.95×10^8 (M.K.S.). At least six plots similar to Fig. 11 were determined for each sample at different temperatures. In all cases, for the samples with 8.0, 19.4 and 27.4 mole % $KNbO_3$, the plots were similar to Fig. 11 with linear dependence of the inverse dielectric constant on the square of the polarization.

The polarization dependence of the dielectric constant of the 38.8 mole % $KNbO_3$ sample is shown in Fig. 12. The graph can be fitted almost exactly with Eq. 18'. The dark circles in Fig. 12 represent data points while the solid curve is a plot of the equation

$$\frac{1}{\kappa} = 7.42 \times 10^{-5} + 1.48 \times 10^{-3} P^2 + 3.44 P^4.$$

Relating this equation to Eq. 18' and noting that $\epsilon = \kappa \epsilon_o$, one finds $B = 0.14 \times 10^8$ and $C = 1.30 \times 10^{10}$ (M.K.S.). This data was taken at 308°K, 6°K above the transition. Figure 12 is characteristic of the

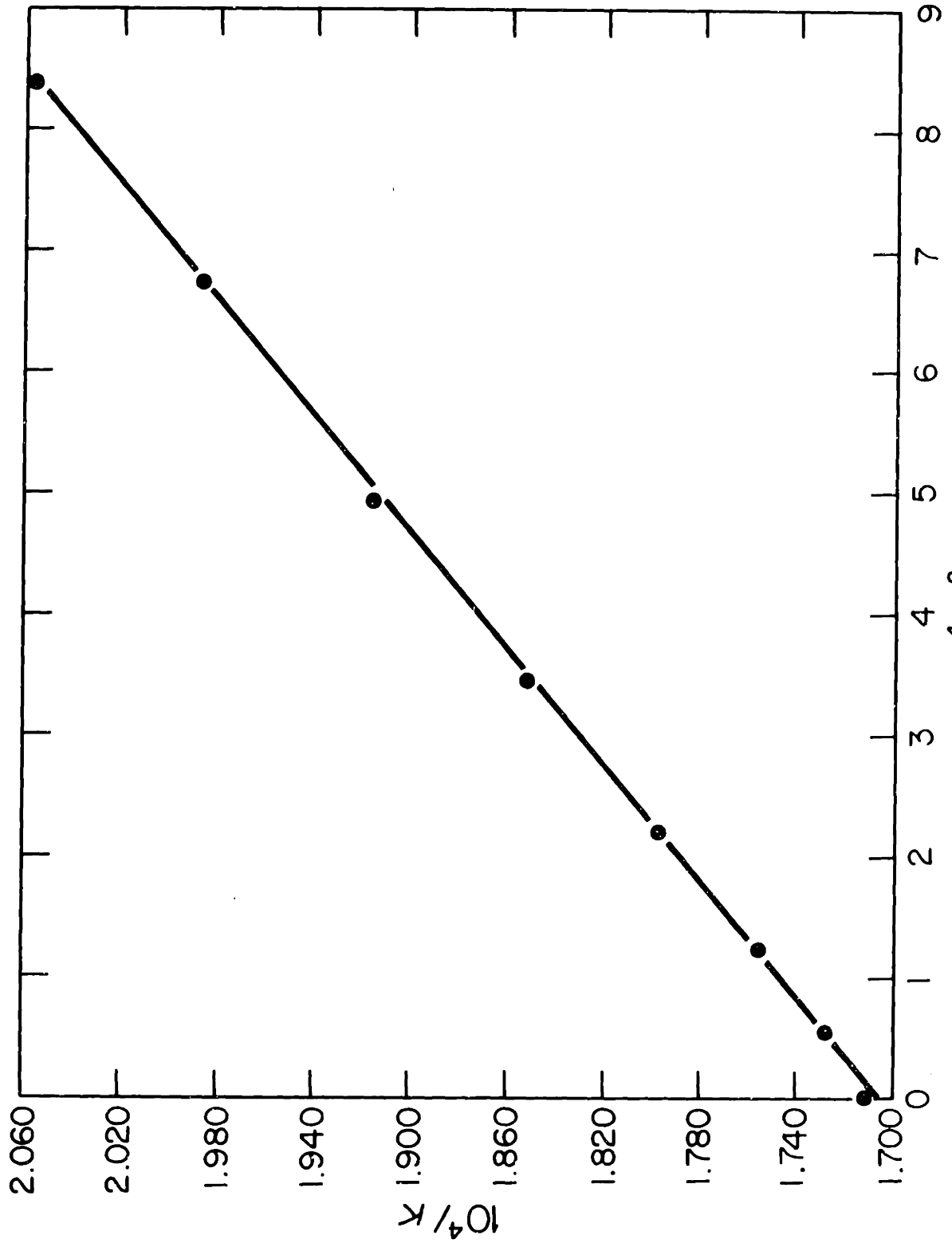

Fig. 11. Polarization dependence of dielectric constant for $KTa_{0.806}Nb_{0.194}O_3$.

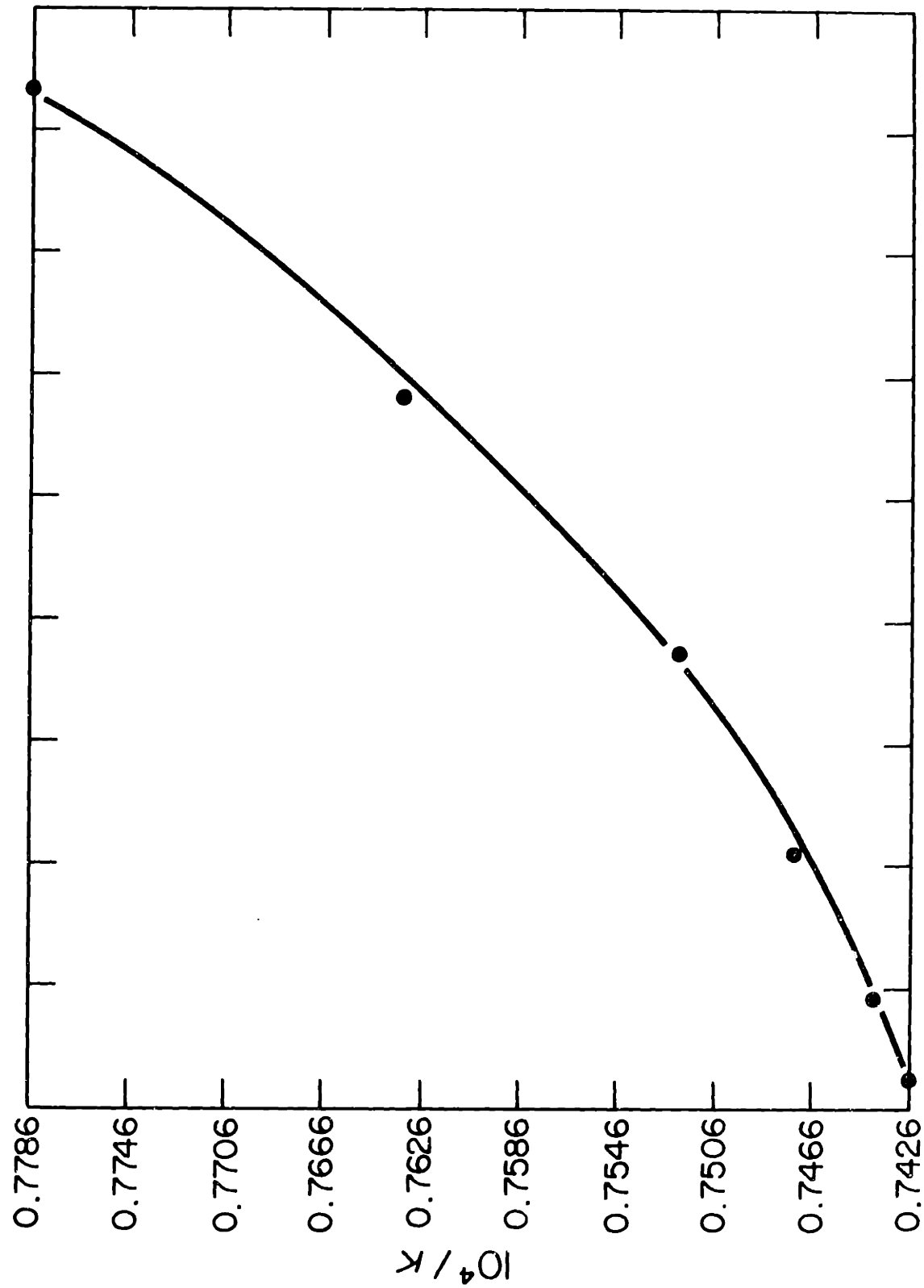

Fig. 12. Polarization dependence of dielectric constant for $KTa_{0.612}Nb_{0.388}O_3$.

data for the 33.2 and 38.8 mole % $KNbO_3$ samples taken at temperatures from 5^o to 15^oK above the transition. Data for these two samples taken at temperatures greater than 15^oK above the transition revealed linear dependence of the inverse dielectric constant on the square of the polarization similar to Fig. 11.

Data was taken at several temperatures for each sample so that the temperature dependence of B could be determined. Figure 13 shows the polarization dependence of the dielectric constant for the 27.4 mole % $KNbO_3$ sample taken at five different temperatures. The ordinate of the graph is $(\frac{1}{\kappa} - \frac{1}{\kappa_o})$, where κ_o is the dielectric constant at zero polarization. The slope is an increasing function of temperature indicating that B is also an increasing function of temperature. A plot of the temperature dependence of B for this sample is shown in Fig. 14. The value of B increases almost linearly over a 10^o to 12^oK range above the transition temperature and then saturates approximately to a constant value. This form of temperature dependence is characteristic of all samples investigated. The increase of B with temperature accounts for the fact that the polarization dependence curves for the 33.2 and 38.8 mole % $KNbO_3$ samples become linear at higher temperatures. At temperatures near the transition for these two compositions, the value of B is quite small and the fourth-order polarization term in Eq. 18' dominates the polarization dependence of the dielectric constant. This results in the nearly parabolic form of Fig. 12. As the temperature increases, the value of B increases and the second-order polarization term in Eq. 18' becomes so large that the fourth-order term in that equation is negligible, thus giving

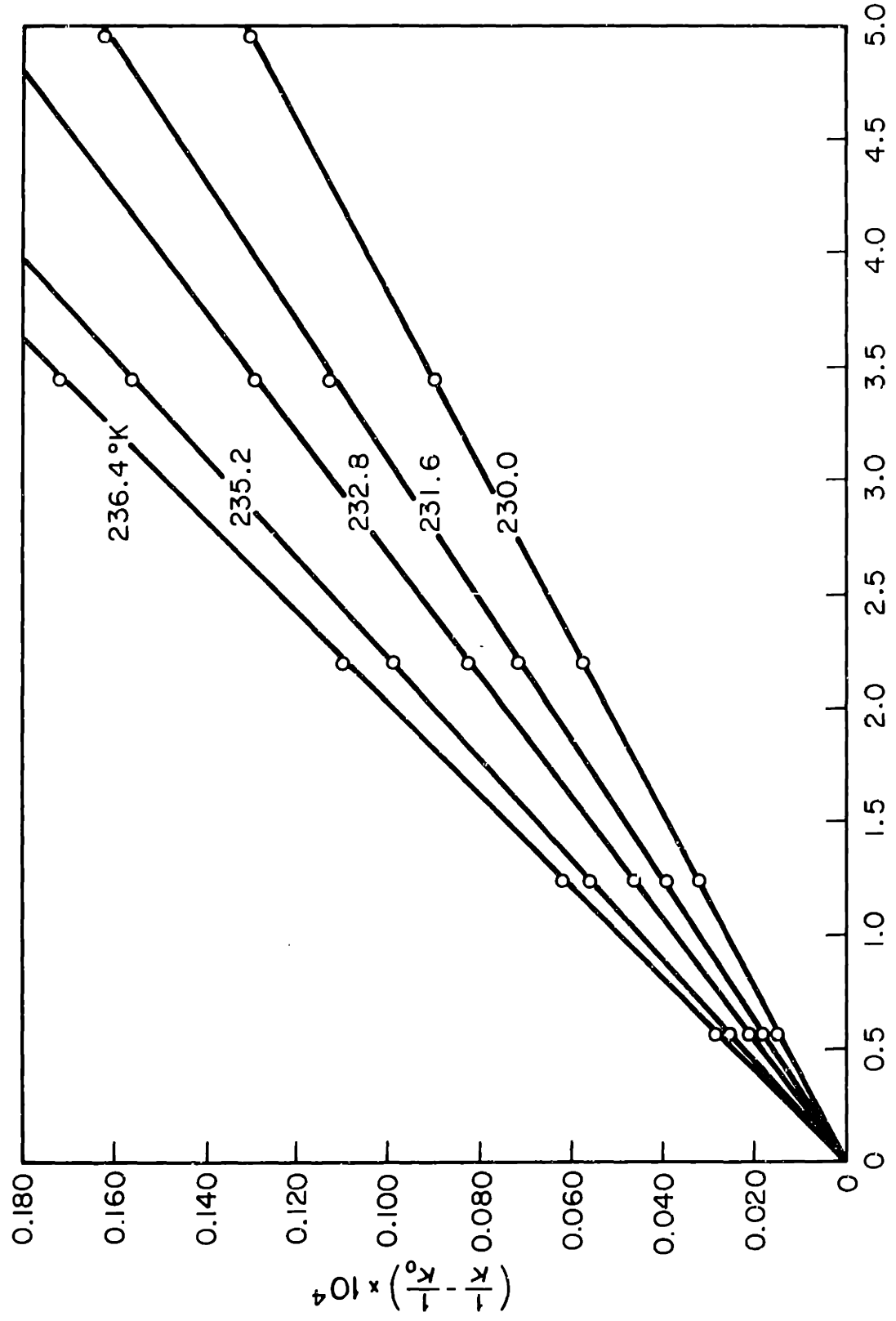

Fig. 13. Polarization dependence of $KTa_{0.726}Nb_{0.274}O_3$ at five temperatures.

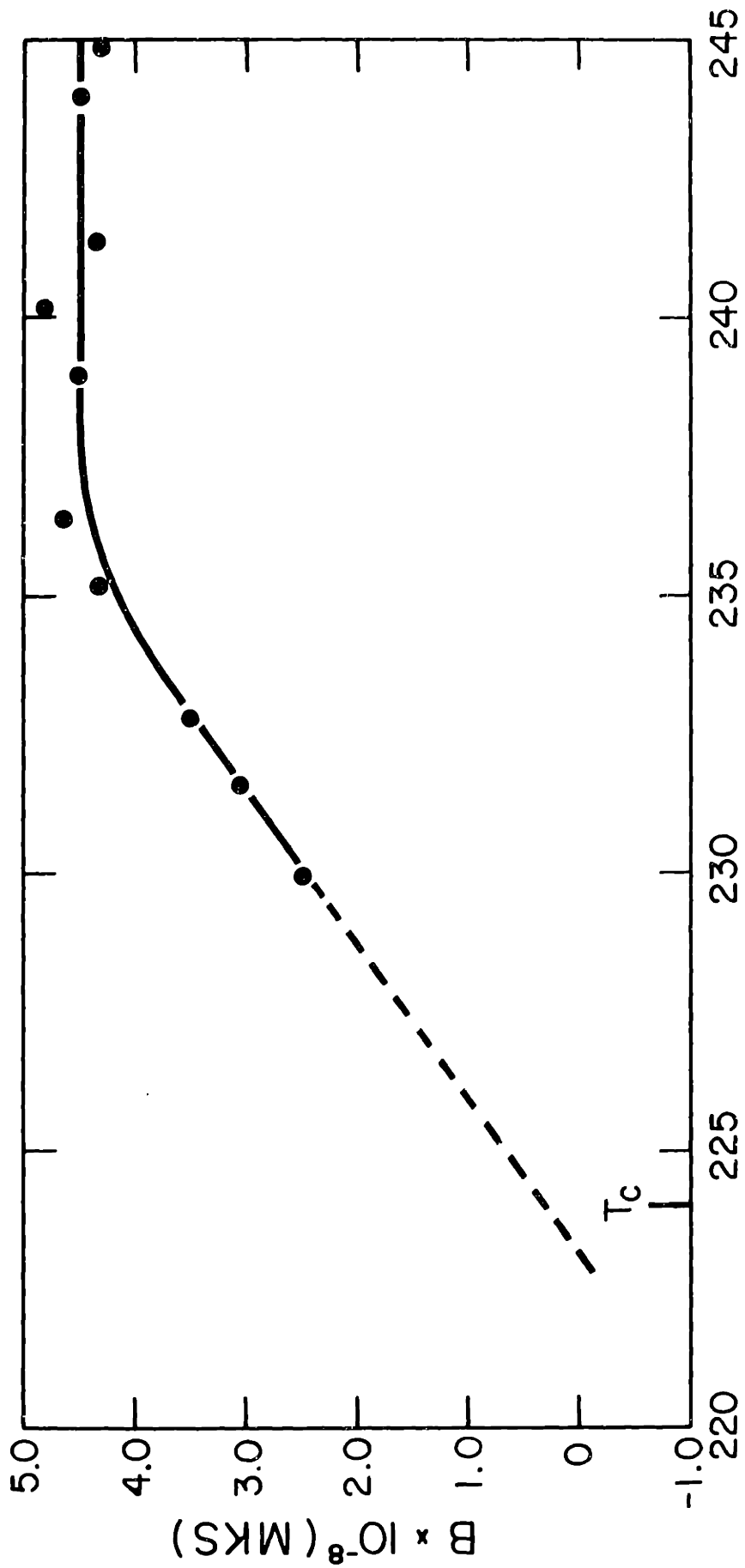

Fig. 14. B vs. temperature for $KTa_{0.726}Nb_{0.274}O_3$.

linear dependence of the dielectric constant on the square of the polarization at temperatures greater than 15°K above the transition.

It was shown in the thermodynamic section that the order of the transition could be determined from the value of B. This determination is quite simple if B is independent of temperature. The value of B measured at any temperature would then decide the order of the transition, a positive value indicating a second-order transition and a negative value, a first-order transition. The determination of the order of the transition is a bit more difficult in the case of KTN since B is not independent of temperature. The value of B may be positive when measured several degrees above the transition but may become negative as the transition temperature is approached. Therefore, in order to determine the order of the transition, it is necessary to know the value of B at the transition. In Fig. 14 this value is 0.33×10^8 at $T_c = 224.0^\circ K$. Since this value is positive, the 27.4 mole % $KNbO_3$ sample has a second-order paraelectric-to-ferroelectric phase transition.

Linear dependence of B on temperature has been reported for $BaTiO_3$ by Landauer, Drougard and Young.[31] The value of B was found to increase over a 30°K temperature range above the transition but there was no saturation of the B term. Their plot of B vs. temperature can be represented by the equation

$$B = 3.64 \times 10^6 \ (T - 448^\circ K).$$

The linear part of the curve in Fig. 14 can be written as

$$B = 3.33 \times 10^7 \ (T - 217^\circ K).$$

These two equations show that the temperature dependence of B, in the linear region, for the 27.4 mole % $KNbO_3$ sample is about a factor of ten larger than the temperature dependence in $BaTiO_3$. Temperature dependence of B in $KTaO_3$ has been reported by Wemple.[21] Only two values of B were measured, one at 4.2°K and the other at 275°K. The value of B was found to decrease with increasing temperature but the exact nature of the temperature dependence was not determined.

A plot of B vs. crystal composition is shown in Fig. 15. The value of B plotted is the value at the paraelectric-to-ferroelectric transition temperature. The composition at which the transition changes from first- to second-order is seen to be 30 mole % $KNbO_3$. Higher $KNbO_3$ concentrations yield negative B values and hence first-order transitions while the compositions below 30 mole % $KNbO_3$ give second-order transitions. The actual dependence of B on composition has not been determined outside of the composition range 8.0 to 40.0 mole % $KNbO_3$, but a dashed line has been drawn to values of B that have been published for $KNbO_3$[14] and $KTaO_3$.[21]

The value of the critical composition found here, 30 mole % $KNbO_3$, differs considerably from the value reported by Triebwasser,[7] 45 mole % $KNbO_3$, and from the value reported by Kurtz,[10] 33 mole % $KNbO_3$. Neither of these values is felt to be very accurate due to the manner in which they were determined. Triebwasser did not determine the order of the transition from measurements of the polarization dependence of the dielectric constant. He attempted to calculate the value of B from Eqs. 16 and 17 of the thermodynamic section. These equations are:

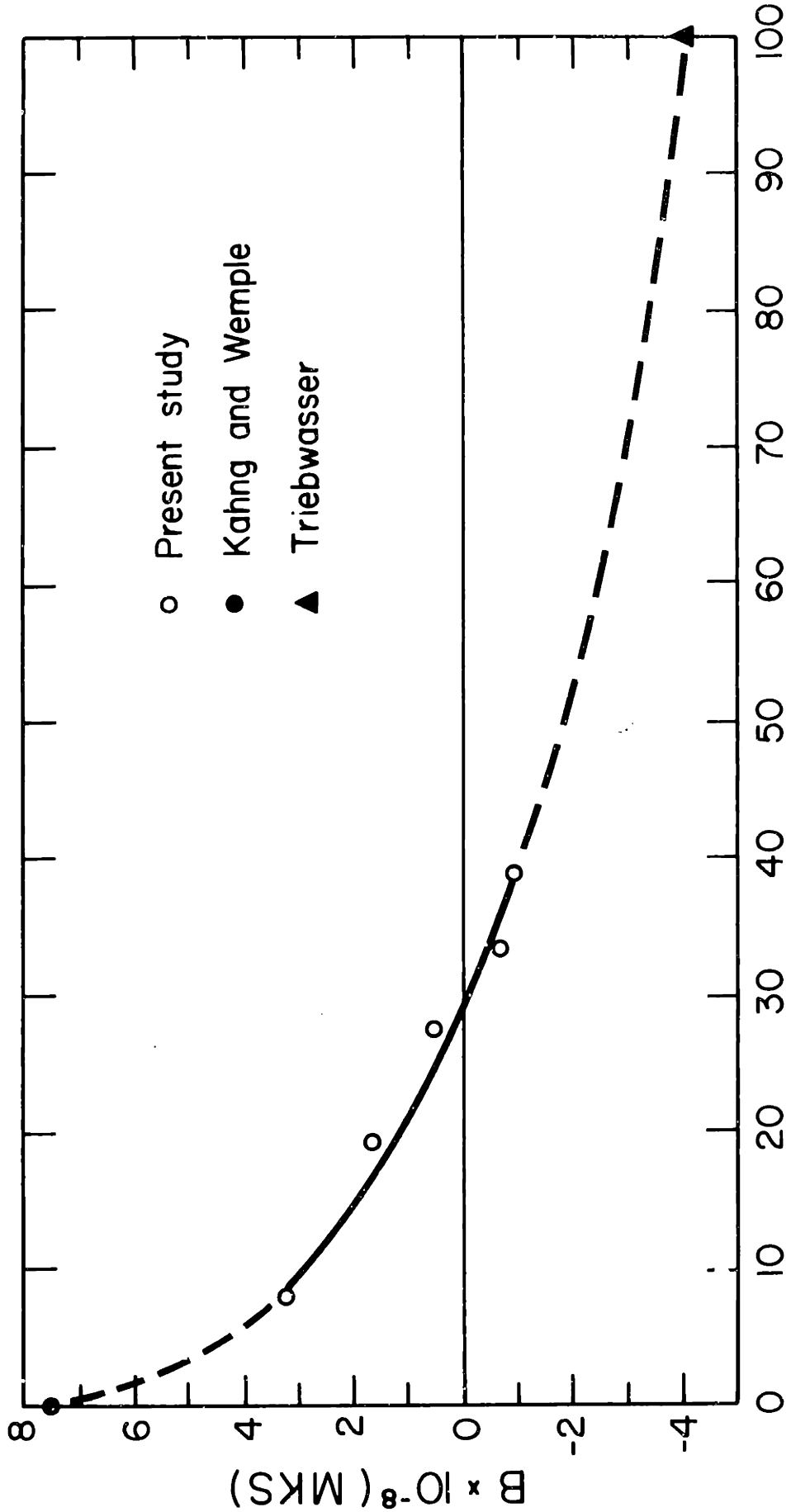

Fig. 15. B vs. composition for the KTN system.

$$P_{tr}^2 = - B/2C \tag{16}$$

$$B^2/4C = A'(T_{tr} - T_o), \tag{17}$$

where P_{tr} is the value of the spontaneous polarization at the transition temperature, T_{tr}, B and C are defined in Eq. 9 and A' and T_o are defined in Eq. 12. Solving these two equations for B, one finds

$$B = -2A'(T_{tr} - T_o)/P_{tr}^2. \tag{45}$$

In order to evaluate B from this expression, it is necessary to calculate the quantity $A'(T_{tr} - T_o)$ from dielectric behavior in the paraelectric phase and also to measure the value of the spontaneous polarization at the transition. Triebwasser did not report any numerical values for B because he could not get any reliable data on the spontaneous polarization due to excessive heating of the samples when hysteresis loops were attempted. He therefore did not use the sign of B to determine the order of the transition but merely observed the temperature dependence of the inverse dielectric constant. From Eqs. 11 and 12, this temperature dependence in the paraelectric phase, P = 0, can be written

$$1/\varepsilon = 2A = 2A'(T - T_o). \tag{46}$$

Also, from the theory section, the transition temperature is equal to the Curie-Weiss temperature, T_o, for a second-order transition and is a few degrees above it for a first-order transition. Therefore, for a second-order transition $1/\varepsilon$ will be approximately zero at the transition and will be greater than zero at a first-order transition. Using this criterion, Triebwasser reports data for only one crystal which

shows a second-order transition. The composition of this sample was 20 mole % $KNbO_3$. The next higher concentration studied contained 46 mole % $KNbO_3$ and was found to have a first-order transition. The determination of the order of the transition using this method is not very accurate; however, his conclusions for these two samples are probably correct since both are located quite far from the critical composition. The only thing that can be concluded from his findings is that the transition changes from first- to second-order somewhere between 20 and 46 mole % $KNbO_3$. The value of 45 mole % $KNbO_3$ as the critical composition seems to have no quantitative validity.

Kurtz's value of 33 mole % $KNbO_3$ as the critical composition is somewhat questionable since this value was extracted from only three data points and as assumed linear dependence of B on composition. He determined two negative values of B at compositions of 36 and 40 mole % $KNbO_3$ and used a value of B for $KTaO_3$ determined by Kahng and Wemple.[21] The value he used for $KTaO_3$ was measured at $275^{o}K$ and was 7.5×10^{8} (M.K.S.). Kahng and Wemple also measured a value of about 22×10^{8} at $4.2^{o}K$. This latter value would be the more appropriate one to use since it would be the one closest to the "transition." If this value had been used, and linear temperature dependence of B again assumed, a value of approximately 36 mole % $KNbO_3$ would have been determined as the critical composition. From Fig. 15, it is evident that the assumption of linear dependence of B on composition is incorrect. The two values of B determined at 36 and 40 mole % $KNbO_3$ agree with the data in Fig. 15.

The value of C in Eq. 18' for the 33.2 mole % $KNbO_3$ sample was approximately 1.5×10^{10} (M.K.S.) near the transition, while this value for

the 38.8 mole % $KNbO_3$ sample was 1.3×10^{10} (M.K.S.) measured 6°K above the transition. The value of C could not be measured accurately for the samples in which B was large because the P^2 term in Eq. 18' was much larger than the P^4 term. Chen et al.[8] report a value of C equal to 1.7×10^8 (M.K.S.) for a sample containing about 38 mole % $KNbO_3$. Also, Triebwasser[14] has calculated a value of C for $KNbO_3$ of 0.30×10^{10} (M.K.S.) from measurements of the spontaneous polarization at the transition and from the temperature dependence of the dielectric constant in the paraelectric phase. Using his value for $KNbO_3$ and the ones determined for lower concentrations of $KNbO_3$, it appears that C decreases with composition.

From Eq. 16 in the section on thermodynamics, the spontaneous polarization at the transition for a crystal having a first-order transition is given by

$$P_s^2 = -B/2C. \tag{16}$$

Using the values of B and C determined for the two first-order samples and Eq. 16, one finds a spontaneous polarization of 4.82×10^{-2} (M.K.S.) for the 33.2 mole % $KNbO_3$ sample and 5.88×10^{-2} (M.K.S.) for the 38.8 % sample. These values seem quite reasonable since the spontaneous polarization at the transition for $KNbO_3$ is 26×10^{-2} (M.K.S.)[14] and since this polarization must decrease to zero at the critical composition, 30 mole % $KNbO_3$, because the transition then becomes second order. Values of the spontaneous polarization at the transition for KTN have not been reported.

2. Raman Scattering Results

Raman scattering was observed in nine crystals with compositions 6.4, 8.0, 9.0, 11.0, 14.0, 19.4, 25.0, 27.4 and 33.2 mole % $KNbO_3$. The critical composition at which the order of the transition changes from first- to second-order was determined to be 30 mole % $KNbO_3$. Since it was desired to study the correlation between the damping of the soft mode and order of the phase transition, the two compositions of most concern were 26.4% and 33.2% $KNbO_3$.

First-order Raman scattering is not allowed in a crystal in which each ion is at a site of inversion symmetry. This is the case for a single compound crystal of the cubic perovskite structure but is not necessarily true for a mixed crystal since inversion symmetry no longer exists. It was found, however, that there was no first-order spectrum in the cubic, nonpolar phase of KTN and thus the symmetry restrictions still apply approximately to this mixed crystal system. The Raman spectrum in the nonpolar phase is a continuous, second-order spectrum, with broad peaks corresponding to a high density of states for two-phonon processes.

The symmetry restriction in the cubic phase can be removed by the method of Fleury and Worlock mentioned in the section concerning experimental techniques. This method was used in the cubic phase of KTN in an attempt to observe the temperature dependence of the soft mode frequency. It was not possible, however, to determine the temperature of the scattering region due to excessive heating of the sample caused by photoconductivity. The mode profiles could, however, be observed and a profile of the soft mode for the 6.4 mole % $KNbO_3$ sample

is shown in Fig. 16. The mode profile can be described quite well by a classical damped harmonic oscillator function. An important observation made during the field-induced scattering measurements was that underdamped modes in the nonpolar phase were also underdamped in the rhombohedral phase, and overdamped modes in the nonpolar phase were overdamped in the rhombohedral phase. Due to the experimental difficulties mentioned above, the damping of the soft mode was studied in the polar phases where the first-order Raman scattering is no longer prohibited by symmetry.

All of the scattering data reported with the exception of Fig. 16, was taken in the polar phase. Therefore, it was necessary to know the symmetry of the polar phase during the scattering experiments. To do this, the capacitance of each scattering sample was measured as a function of temperature to determine the exact temperature of the phase transitions. There was, however, a slight problem due to the heating of the sample by the laser. During the experiment, an optical attenuator was placed in the laser path as the excitation line was scanned. When the scattering reached a tolerable level, the attenuator was removed and the laser light incident on the sample caused the capacitance to decrease. To see the effect of this heating, the capacitance was measured for the 11.0 mole % $KNbO_3$ sample with and without the laser. These results are shown in Fig. 17. The data was taken as the sample was cooling in both cases in order to avoid the effect of thermal hysteresis. The laser causes a maximum heating of about one degree and the effect is therefore not important.

The soft mode was found to be overdamped in the tetragonal and ortho-

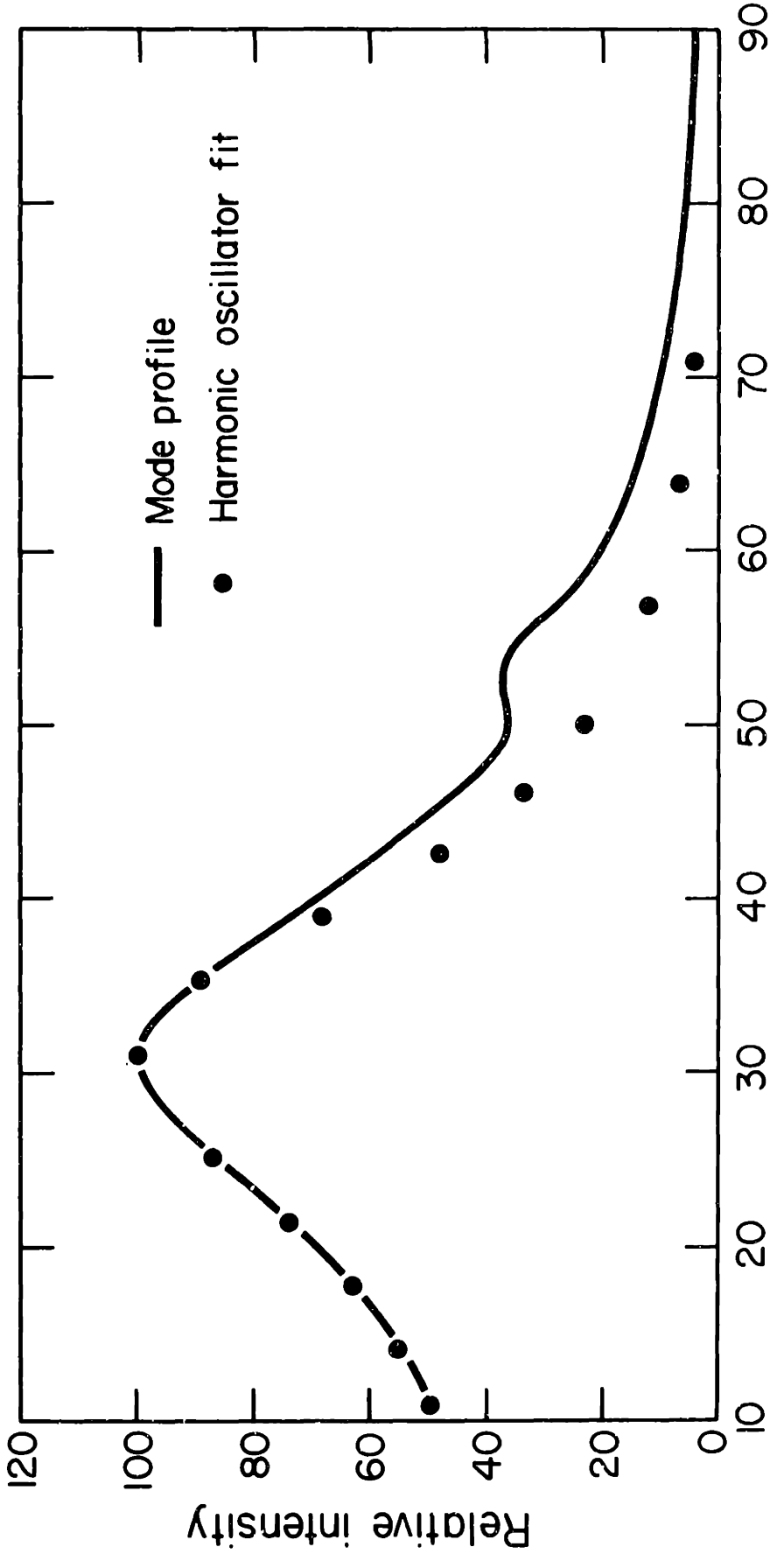

Fig. 15. Field-induced scattering for $KTa_{0.935}Nb_{0.064}O_3$.

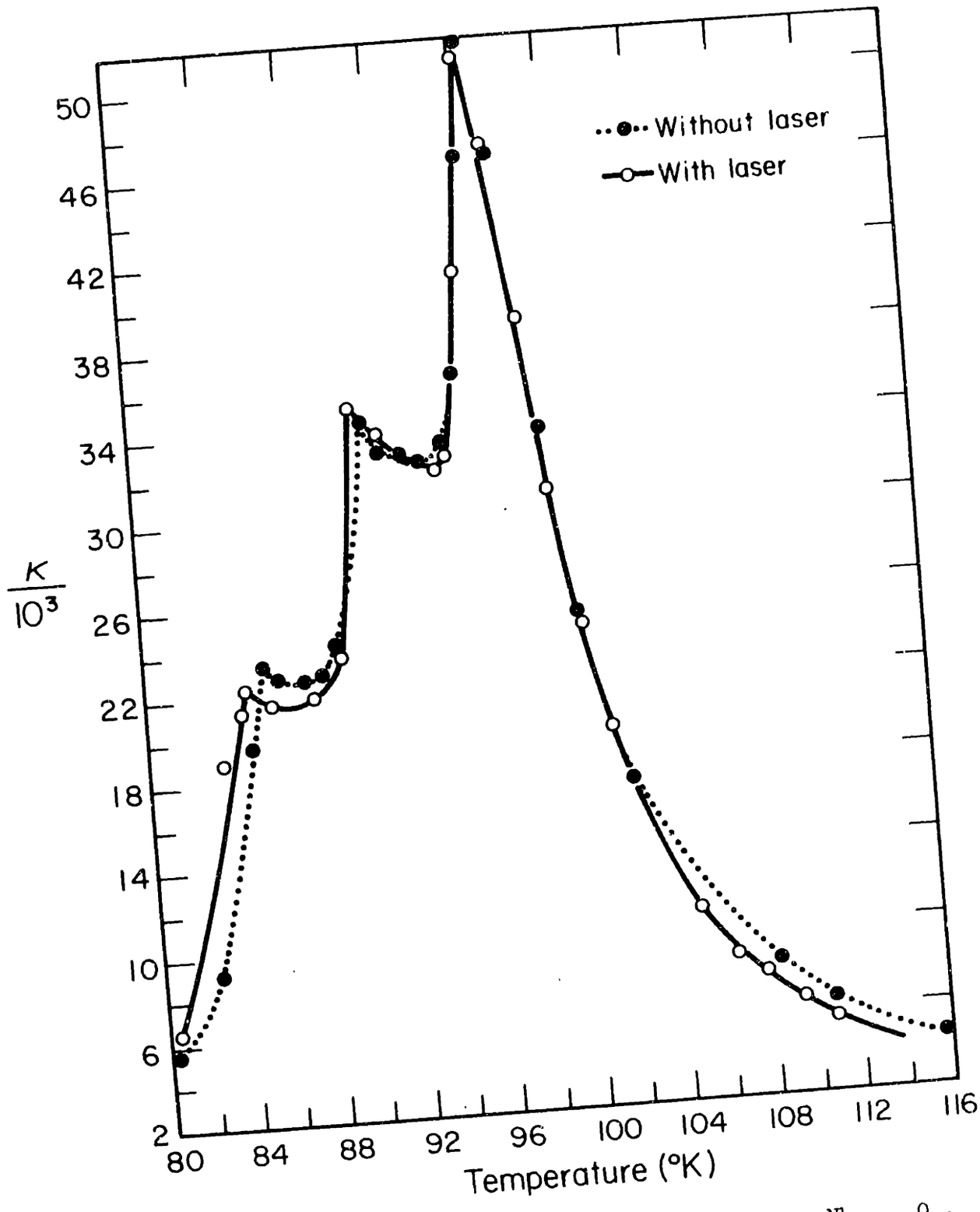

Fig. 17. Dielectric constant measurements for $KTa_{0.890}Nb_{0.110}O_3$.

rhombic phases for all of the KTN crystals studied. The only underdamped soft modes observed were in the rhombohedral phase. In this phase, for the lower compositions, the mode was relatively narrow with a width of approximately 20 cm^{-1}. For temperatures well below the lowest symmetry phase transition, the mode profile appeared to be a single underdamped mode. As the temperature increased toward the transition, however, the profile became quite unsymmetrical indicating possible mode splitting. For the compositions above 11.0 mole % $KNbO_3$, two modes could be resolved. The higher frequency mode was temperature dependent and disappeared at the rhombohedral-orthorhombic transition. The lower frequency mode showed no temperature dependence in the rhombohedral phase. It was observable in the orthorhombic phase but was still temperature independent. Eventually the mode peak was masked by the intense scattering from the overdamped mode in the orthorhombic phase. The temperature dependence of the soft mode was observed over a wide temperature range for several compositions. This data is shown in Fig. 18 for the compositions 6.4, 8.0 and 9.0 mole % $KNbO_3$. The mode peaks were only observable to within 15 cm^{-1} of the excitation line so that the behavior of the mode is not known below this value. A dashed line has been extrapolated to the temperature at which the lowest temperature phase transition occurs. The mode frequency need not go to zero, since the orthorhombic-rhombohedral transition must be first-order. A considerable temperature dependence of the mode is observed in the 6.4% $KNbO_3$ sample. It appears that the mode is quite "soft" at the lowest temperature transition. The mode shows less temperature dependence with increasing niobium concentration where it disappears

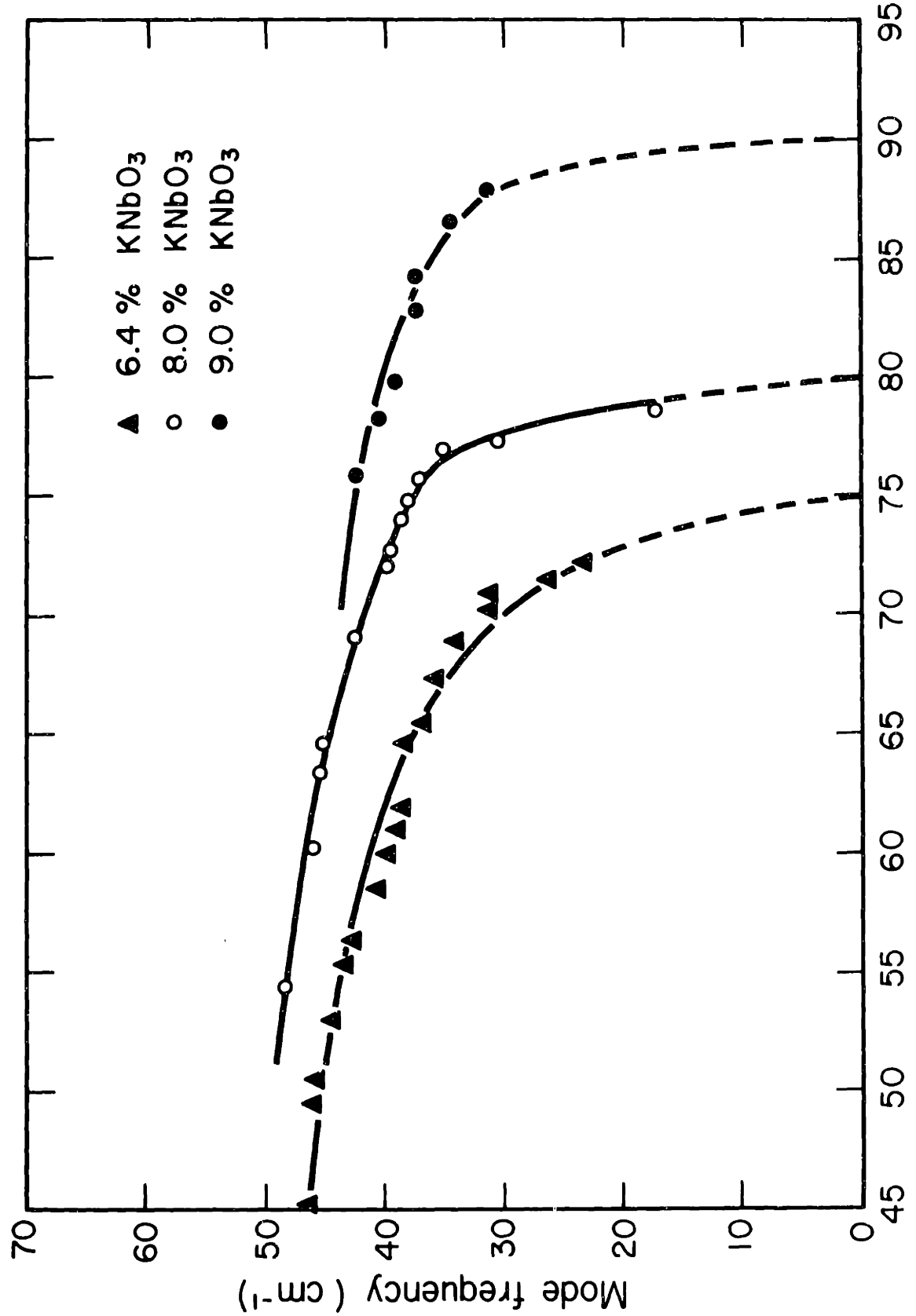

Fig. 18. Temperature dependence of soft mode for three KTN samples.

abruptly at the transition. Figure 19 shows the temperature dependence of both of the resolved modes for the composition 25.0 mole % $KNbO_3$. Within the limits of the experiment, the mode frequencies are temperature independent, but the scattering disappears abruptly at the lowest transition temperature, which is 178°K for this composition.

The damping of the soft mode was the most important characteristic in this study since it was desired to study the correlation between the damping and the order of the phase transition. It was found that the damping generally increased with increasing $KNbO_3$ concentration. The mode for the 6.4% $KNbO_3$ sample was quite narrow with a width of approximately 20 cm^{-1}, while the mode was about 65 cm^{-1} wide for the 27.4% $KNbO_3$ sample. The modes for the 14.0 and 27.4% $KNbO_3$ samples are shown in Figs. 20 and 21, respectively. The peaks in these two spectra at 120 cm^{-1} and 128 cm^{-1} correspond to strong second-order scattering. It has been observed in the nonpolar phase with no applied fields over a fifty degree temperature range and showed no temperature dependence. This mode appears to increase in energy with increasing $KNbO_3$ concentration.

From the dielectric study, it was found that the critical composition was 30 mole % $KNbO_3$, which has a paraelectric-to-ferroelectric transition at 225°K. The 27.4% $KNbO_3$ scattering sample was the highest temperature second-order transition observed. On the other side of the critical composition was the 33.2% $KNbO_3$ sample. The mode profile for the 27.4% $KNbO_3$ sample is shown in Fig. 21. It is heavily damped but clearly not overdamped. In the case of the 33% sample, the soft mode was found to be overdamped in all phases. The soft mode does

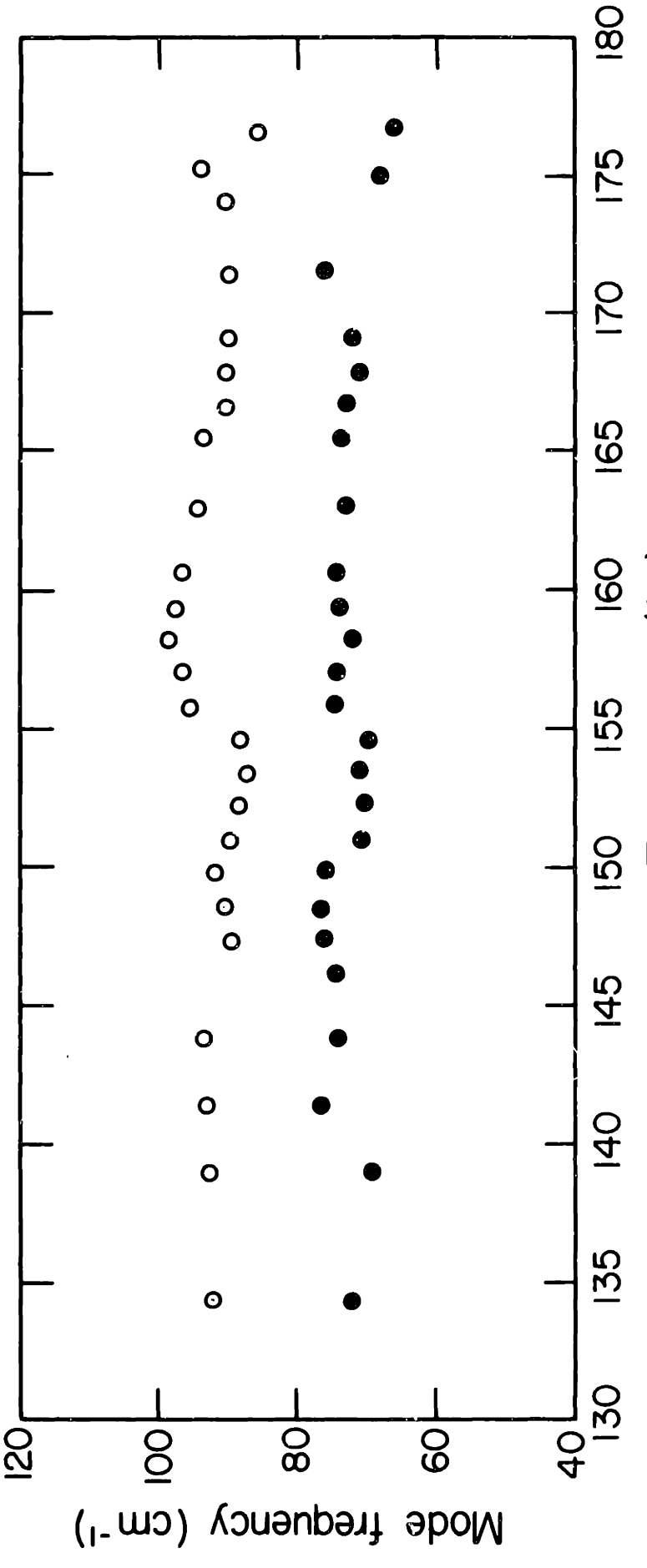

Fig. 19. Temperature dependence of modes for $KTa_{0.750}^{Nb}{}_{0.250}O_3$.

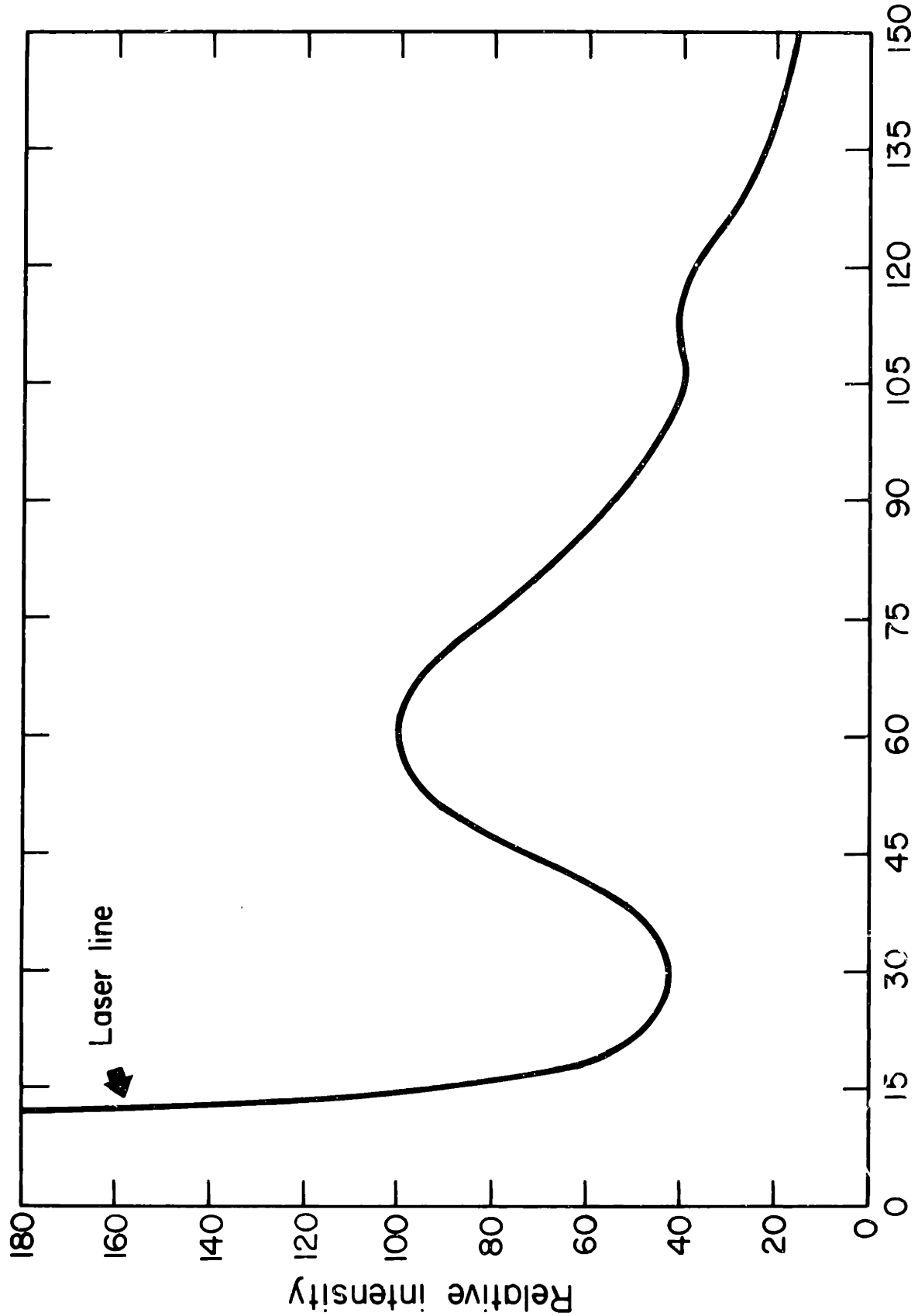

Fig. 20. Soft mode profile for $KTa_{0.860}Nb_{0.140}O_3$.

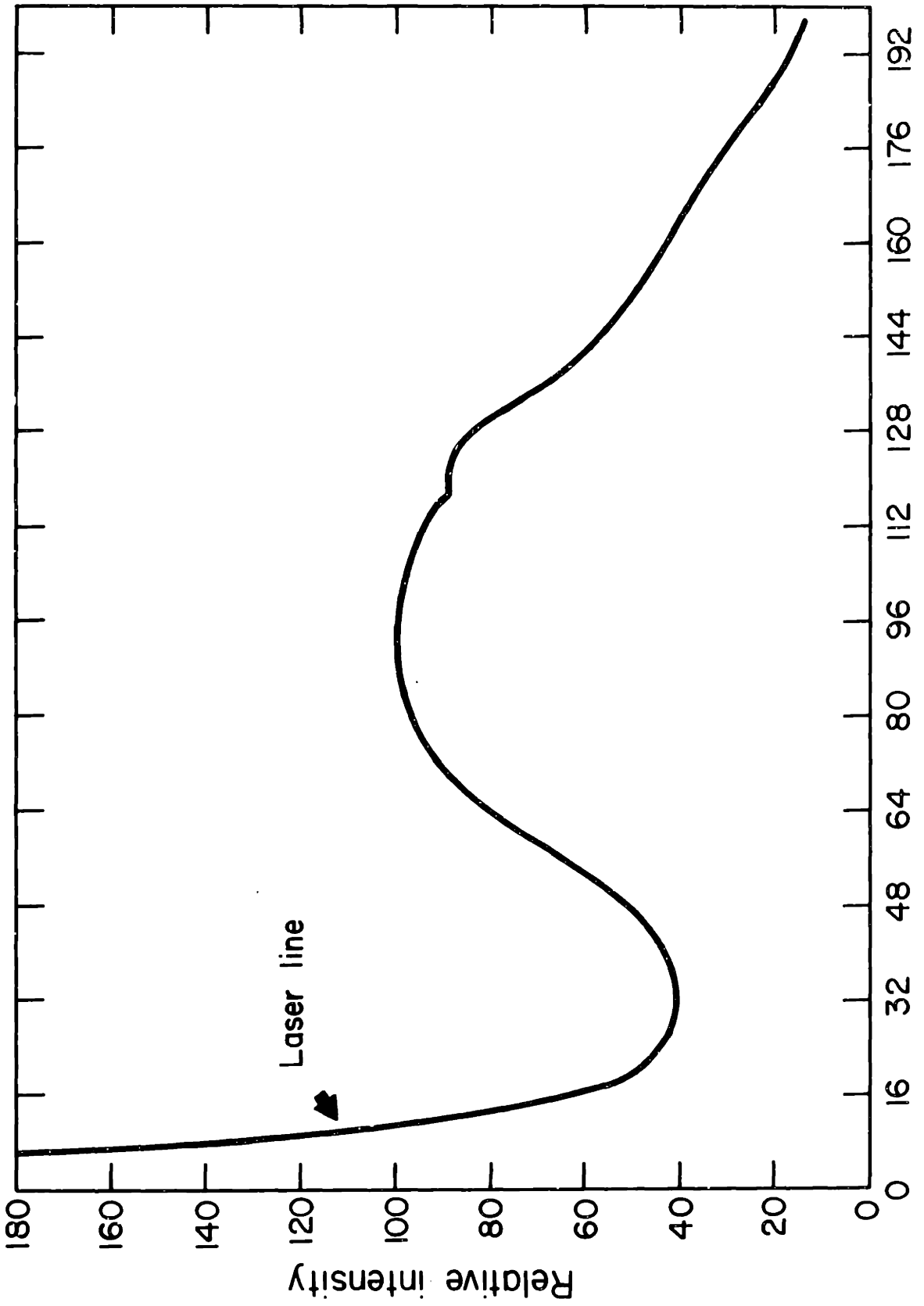

Fig. 21. Soft mode profile for $KTa_{0.726}Nb_{0.274}O_3$.

not show a peak but appears as a broad shoulder on the excitation line. Figure 22 shows the observed Raman spectrum in the cubic and tetragonal phases. For compositions greater than 33% $KNbO_3$, the scattering spectra were similar to Fig. 22.

The above observations demonstrate a strong correlation between the damping of the mode and the thermodynamic order of the paraelectric-to-ferroelectric transition. It is felt that this correlation is not merely accidental since the soft mode in $BaTiO_3$, which has a first-order transition, is heavily overdamped while this mode is underdamped for all compositions of the mixed crystal system $(Na,K)TaO_3$, which has a second-order transition for all compositions.

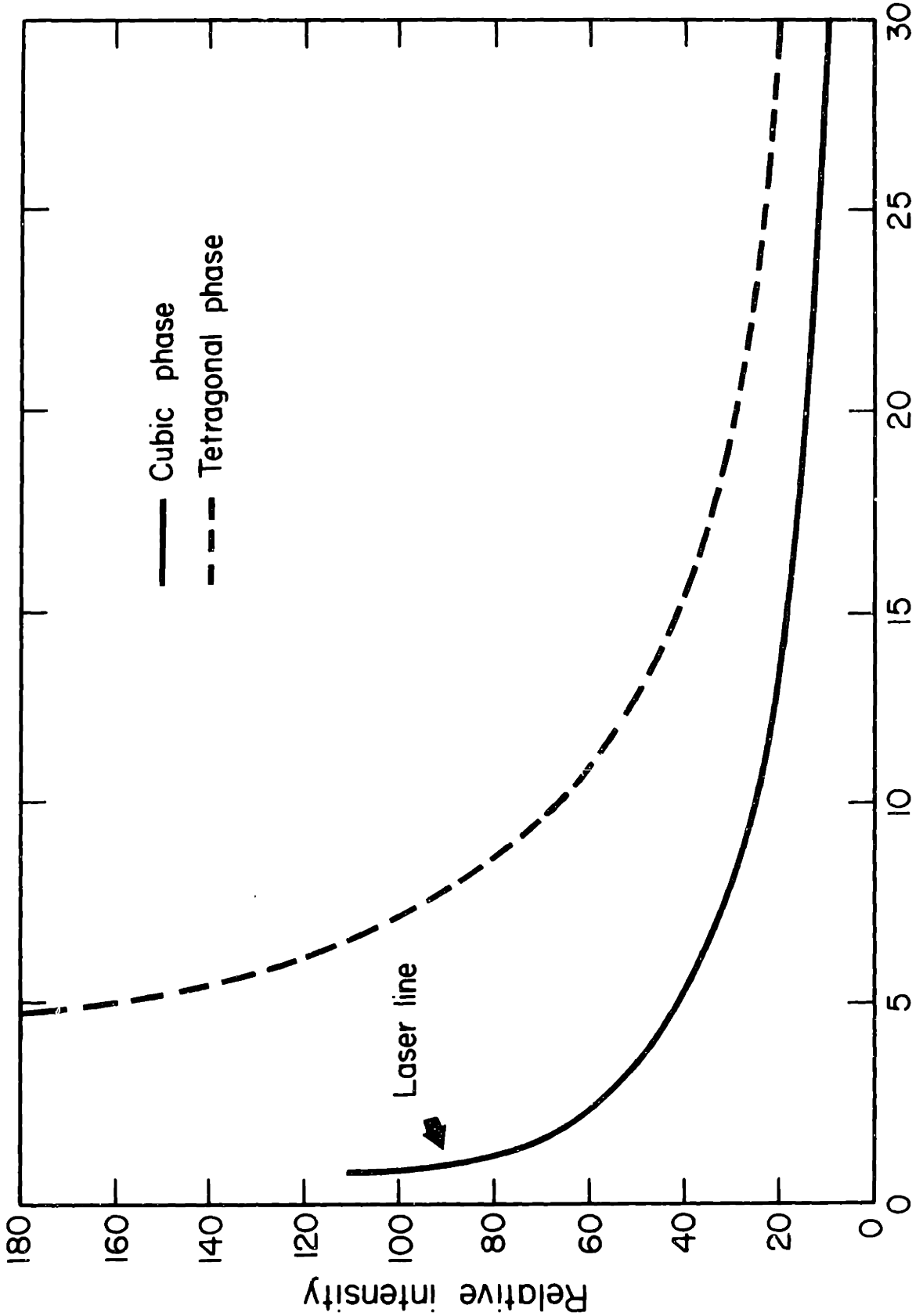

Fig. 22. Scattering from overdamped mode in tetragonal phase of $KTa_{0.670}Nb_{0.330}O_3$.

V. SUMMARY AND CONCLUSIONS

The observed features of the KTN system are briefly the following: The order of the paraelectric-to-ferroelectric transition changes from first- to second-order at a concentration of 30 mole % $KNbO_3$ with higher niobium concentration giving first-order transitions and lower concentrations, second-order transitions. The fourth-order polarization coefficient in the Devonshire free energy expansion is linearly temperature dependent over a ten to twelve degree range above the transition temperature and saturates to a constant value at higher temperatures. The temperature dependence in the linear region is about ten times that reported for $BaTiO_3$. The sixth-order polarization coefficient in the free energy expansion gives a large contribution to the polarization dependence of the dielectric constant near the critical composition. The value of this coefficient appears to decrease with increasing $KNbO_3$ concentration. The values of the fourth- and sixth-order polarization coefficients determined give quite reasonable values for the spontaneous polarization at the transition temperature.

The ferroelectric soft mode was found to be underdamped for compositions below 30 mole % $KNbO_3$, the critical composition. Above this concentration, the soft mode was overdamped in all phases. The underdamped soft mode appeared only in the rhombohedral phase and all modes in the orthorhombic and tetragonal phases were overdamped. The soft mode in the rhombohedral phase showed a considerable temperature dependence for the $KTa_{0.94}Nb_{0.06}O_3$ sample but showed less temperature dependence with increasing niobium concentration. Near

the critical composition, the mode appears temperature independent but disappears abruptly at the lowest transition temperature. The mode profile in KTN can be fitted to a classical damped harmonic oscillator function. Although a damped harmonic oscillator function is often assumed for the line shape, this is by no means a general feature of heavily damped modes. In the mixed crystal system $(K,Na)TaO_3$, the soft mode profiles were not at all well described by harmonic oscillator functions.[6]

A major accomplishment of this work was the use of a low duty factor AC bias technique to measure the polarization dependence of the dielectric constant. This method allowed an accurate determination of the coefficients in the free energy expansion without heating the sample, a problem which is encountered in other techniques.

The dependence of the transition temperatures on composition was determined for the composition range five to sixty mole percent $KNbO_3$. It was found that the three transitions became closer together with decreasing niobium concentration and that only one transition is observed at approximately five mole percent $KNbO_3$. The dependence of the crystal composition on the melt composition was also determined.

The only thing considered in the theoretical section which could explain the change in the order of the transition is that the sign of the coefficient of the fourth-order anharmonic term in the ion potential change from positive to negative. It must therefore be a function of the crystal composition. Since the only change in the crystal is the concentration of the tantalum and niobium atoms, this

coefficient may be a function of the polarizability of the two ions and the dimensions of the unit cell, the structure for $KTaO_3$ and $KNbO_3$ being slightly different.

Further work in this area should concentrate on a model which will explain the observed effects. The fact that KTN is a mixed crystal system complicates this problem. A proper treatment of the random location of the tantalum and niobium ions must first be determined. A first approximation would be to assume an average polarizability of the center ion in the perovskite structure and apply the Slater model to see if the observed dielectric data could be explained.

No hypothesis can be made at the present time with regard to the correlation between the damping of the ferroelectric mode and the order of the paraelectric-to-ferroelectric transition. An appropriate model for the dielectric data would necessarily contain information about the soft mode but would probably not be sufficient to explain the damping of the mode.

The two primary goals of the experiment have been achieved: the composition at which the order of the transition changes was determined to be 30 mole % $KNbO_3$ and a correlation between the damping of the soft mode and the order of the transition was found.

APPENDIX

Chemical Analysis

The KTN samples were chemically analyzed by the volumetric method of Headridge and Taylor.[38] Briefly, the method is as follows: Between 200 and 400 mg of sample is dissolved in HF. The acid content of this solution is adjusted to about 0.5 M HF and 6 M HCl. This solution, containing Nb(V) is passed through a Jones reductor to effect reduction to Nb(III). This is extremely sensitive to air oxidation, and the reductor effluent is, therefore, collected in a solution of Fe(III). An amount of Fe(II) equivalent to Nb(III) is formed. The Fe(III) formed is then titrated with standard $K_2Cr_2O_7$ solution. The volume of $K_2Cr_2O_7$ used is linearly proportional to the amount of Nb in the original sample. Pure Nb_2O_5 was used to standardize the method. An accuracy and precision of about $\pm$0.5% was obtained. An air-tight polyethylene apparatus was constructed for the analysis.

REFERENCES

1. Slater, J. C., Phys. Rev. 78, 748 (1950).
2. Anderson, P. W., in Fizika Dielektrikov, Akademiya Nauk, Fisicheskii Inst. i,. P. N. Lebedeva, Moscow, 1960.
3. Cochran, W., Advances in Physics 9, 387 (1960).
4. Lyddane, R. H., R. G. Sachs, and E. Teller, Phys. Rev. 59, 673 (1941).
5. DiDomenico, M., S. P. S. Porto, and S. H. Wemple, Phys. Rev. Letters 19, 855 (1967).
6. Davis, T. G., Ph.D. Thesis, Massachusetts Institute of Technology, Cambridge, Mass., 1968.
7. Triebwasser, S., Phys. Rev. 114, 63 (1959).
8. Chen, F. S., J. E. Geusic, S. K. Kurtz, J. G. Skinner, and S. H. Wemple, J. Appl. Phys. 37, 388 (1966).
9. Wemple, S. H., D. Kahng, C. N. Berglund, and L. G. Van Uitert, J. Appl. Phys. 38, 799 (1967).
10. Kurtz, S. K., Bell Syst. Tech. Journal 8, 1209 (October 1966).
11. Perry, C. H., N. E. Tornberg, in Light Scattering Spectra of Solids, G. B. Wright, Ed., Springer-Verlag, New York Inc., 1969, p. 467.
12. Matthias, B. T., J. P. Remeika, Phys. Rev. 82, 727 (1951).
13. Shirane, G., H. Danner, A. Pavlovic, and R. Pepinsky, Phys. Rev. 93, 672 (1954).
14. Triebwasser, S., Phys. Rev. 101, 993 (1956).
15. Wood, E. A., Acta Cryst. 4, 353 (1951).
16. Vousden, P., Acta Cryst. 4, 373 (1951).
17. Cotts, R. M., W. D. Knight, Phys. Rev. 96, 1285 (1954).
18. Hulm, J. K., B. T. Matthias, and E. A. Long, Phys. Rev. 79, 885 (1950).

19. Wemple, S. H., Ph.D. Thesis, Massachusetts Institute of Technology, Cambridge, Mass., 1963.

20. Wemple, S. H., Phys. Rev. 137, A1575 (1965).

21. Kahng, D., S. H. Wemple, Phys. Rev. 36, 2925 (1965).

22. Devonshire, A. F., Advances in Physics 10, 86 (1954).

23. Fröhlich, H., Theory of Dielectrics, Clarendon Press, Oxford, 1949.

24. Woods, A. B. D., W. Cochran, and B. N. Brockhouse, Phys. Rev. 119, 980 (1969).

25. Leibfried, G., in Encyclopaedia of Physics, Vol. 7, S. Flügge,Ed., Part I, Springer-Verlag, Berlin, Germany, 1955.

26. Barker, A. S. and M. Tinkham, Phys. Rev. 125, 1527 (1962).

27. Ballantyne, J. M., Phys. Rev. 136, A429 (1964).

28. Perry, C. H. and T. F. McNelly, Phys. Rev. 154, 456 (1967).

29. Miller, R. C. and W. G. Spitzer, Phys. Rev. 129, 94 (1963).

30. Kaminow, I. P. and T. C. Damen, Phys. Rev. Letters 20, 1105 (1968).

31. Drougard, M. E.,R. Landauer, and D. R. Young, Phys. Rev. 98, 1010 (1955).

32. Triebwasser, S., Phys. Rev. 118, 100 (1960).

33. Chynoweth, A. G., Phys. Rev. 102, 705 (1956).

34. Merz, W. J., Phys. Rev. 91, 513 (1953).

35. Banks, E. and A. Reisman, J. Am. Chem. Soc. 80, 1877 (1958).

36. Worlock, J. M. and P. A. Fleury, Phys. Rev. Letters 19, 1176 (1967).

37. Reisman, A., S. Triebwasser and F. Holtzberg, J. Am. Chem. Soc. 77, 4228 (1955).

38. Headridge, J. B. and M. S. Taylor, Analyst 87, 43 (1962).